

AD91371

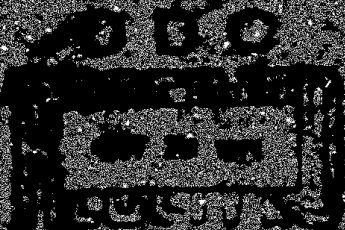
UNITED STATES OF AMERICA

Department of Defense

OFFICE OF THE SECRETARY OF DEFENSE

WASHINGTON, D.C.

20301



RECEIVED

NOV 1964

AD91371

[illegible]

**PERFORMANCE SYNTHESIS OF
ELECTRO-OPTICAL SENSORS**

**Frederick A. Rosell
Robert H. Willson**

**Distribution limited to United States Government agencies only;
test and evaluation 31 August 1973. Other requests for this
document must be referred to Air Force Avionics Laboratory
(NVA-698DF), Wright Patterson Air Force Base, Ohio 45433**

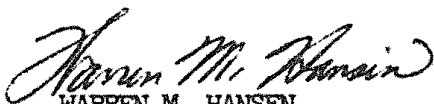
FOREWORD

This program involved the refinement of mathematical models and performance of psychophysical experiments as part of the continuation effort of the 698DF development project for a high-resolution low-light-level television system for tactical airborne application. These studies have led to a better understanding of motion and MTF effects of electro-optical sensors and the use of the results can lead to more realistic system specifications and a reduced need for costly laboratory and flight testing of systems.

The Air Force Project Director on this program was Frank A. McCann, AFAL/NVA(698DF). The Westinghouse effort was conducted principally by Frederick A. Rosell and Robert H. Willson. The program was performed by the Westinghouse Systems Development Division, Baltimore, Maryland, under Air Force Contract F33615-70-C-1461.

This report was submitted by Frederick A. Rosell and Robert H. Willson.

This technical report has been reviewed and is approved for publication.



WARREN M. HANSEN
Acting Deputy Director
Navigation & Weapon Delivery Division

ABSTRACT

This effort is a continuation of the Performance Synthesis Study, Electro-Optical Sensors reported in Technical Report AFAL-TR-72-229, dated August 1972. Analytical models were further developed and refined to include image motion and aperturing effects. Psychophysical experiments were performed as tests of the theories and it was found that the theory is reasonably accurate. A concept of balanced resolution is discussed which combines a system's performance for both aperiodic and periodic imagery. The question of a single figure of merit for a system is also discussed.

TABLE OF CONTENTS

<u>Section</u>	<u>Page</u>
I INTRODUCTION AND SUMMARY	1
II RANGE ANALYSIS AND MODEL UPDATE.	9
2.1 The Sensors Model and Observer Requirements.	9
2.2 Passive Television Imaging System.	27
2.3 Active Television Imaging Systems.	45
2.4 Effects of Image Motion.	49
2.5 The Balanced Resolution Concept.	75
III DISPLAY SIGNAL-TO-NOISE RATIO FUNDAMENTALS	81
3.1 The Elementary Model	81
3.2 The Effect of Finite Apertures on Image Detail	89
3.3 Effect of Apertures on Signal-to-Noise Ratio	118
IV EFFECTS OF IMAGE MOTION.	121
4.1 Psychophysical Experiments Involving Image Motion.	122
4.2 Analysis of Sensor Motion Data	129
V PSYCHOPHYSICAL EXPERIMENTS INVOLVING SENSOR MTF.	139
VI FIGURE OF MERIT.	167
6.1 MTF Related Image Quality Parameters	168
6.2 Signal-to-Noise Ratio Related Image Quality Parameters	175
REFERENCES	180

LIST OF ILLUSTRATIONS

<u>Figure</u>		<u>Page</u>
1	Location of Points of Noise Insertion Relative to the MTF's.	14
2	Video Output Waveforms for a Single Isolated Bar and a Repetitive Bar Pattern.	18
3	Levels of Object Discrimination. Object Area to be Used in the SNR_D Calculations is Δy by L	22
4	Equivalent Bar Pattern Criteria for Object Identification.	22
5	Probability vs Normalized SNR_{DI} . For Any Probability Value. Obtain SNR_{DI} from Table 3 for 50% Probability. Find Value of k for Desired Probability and Multiply Value of SNR_{DI} by k to Obtain New Values of SNR_{DI}	26
6	MTF and MTF Related Function for the Assumed Sample System.	29
7	Display Signal-to-Noise Ratio vs Spatial Frequency for the Assumed System at Various Average Input Photocathode Currents for Bar Pattern Images.	30
8	Display Signal-to-Noise Ratio vs Spatial Frequency for the Assumed System at Various Average Input Photocathode Currents for Aperiodic Images.	31
9	Threshold Resolution vs Average Input Photocurrent for the Assumed System with Input Image Modulation Contrast of 1.0	33
10	Threshold Resolution vs Average Input Photocurrent for the Assumed System with Input Modulation of 0.1	34
11	Threshold Angular Resolution vs Average Input Photocurrent for the Assumed System with Various Input Image Modulation Contrasts. Threshold Resolution is Based on the Balanced Resolution Concept. Angle Corresponds to One Line Width	38

<u>Figure</u>		<u>Page</u>
12	Ratio of Apparent to Inherent Contrast vs Range for Various Values of Sky-to-Ground Ratio for a Meteorological Visibility of 10 Nautical Miles.	42
13	Ratio of Image Contrast at Range R to that at Range Zero for a Meteorological Visibility of 20 Nautical Miles and Sky-to-Ground Ratios of 1.4 and 7.0	42
14	Threshold Resolution vs Range for a Meteorological Visibility of 20 Nautical Miles and Sky-to-Ground Ratios of 1.4 and 7.0	43
15	Threshold Angular Resolution vs Range for a Meteorological Visibility of 20 Nautical Miles and Sky-to-Ground Ratios of 1.4 and 7.0	43
16	Threshold Angular Resolution for Bar Patterns vs Range for the Assumed TV Camera as a Function of Input Image Contrast for a 20 nmi Visibility and a Sky/Ground Ratio of 1.4	44
17	Threshold Angular Resolution for Bar Patterns vs Range for the Assumed TV Camera as a Function of Input Image Contrast for a 20 nmi Visibility and a Sky/Ground Ratio of 7.0	44
18	Average Input Photocurrent for the Assumed System vs Range for an Average Scene Reflectivity of 0.3	47
19	MTF and MTF Related Quantities for the 16/16/16 mm I-EBSICON Camera Used in the Assumed System	48
20	Display Signal-to-Noise Ratio vs Spatial Frequency for the Assumed Active System for an Inherent Image Contrast of 0.5 and a Visibility of 20 nmi. Calculations are based on the Aperiodic Image Model.	50
21	Display Signal-to-Noise Ratio vs Spatial Frequency for the Assumed Active Systems for an Inherent Image Contrast of 0.5 and a Visibility of 20 nmi Calculations Based on the Periodic Image Model.	51
22	Threshold Resolution in Lines/Pict. Ht. for the Assumed Active System vs. Range. Inherent Image Contrast is 0.5	52

<u>Figure</u>		<u>Page</u>
23	Threshold Resolution in Angular Subtense of a Single Line vs Range for the Assumed Active System. Inherent Contrast is 0.5.	52
24	Effect of Image Motion on Bar Patterns of Various Spatial Frequencies.	56
25	Modulation Transfer Function Due to Linear Image Motion Plotted to Second Zero for Various Bar Pattern Velocities Expressed in Terms of Time for Pattern to Transverse Picture Width.	58
26	Spatial Frequency and the Corresponding Angular Motion for the Assumed System for which the Signal Modulation is Zero as a Function of Bar Pattern Motion (Linear).	59
27	Modulation Transfer Function Due to Linear Image Motion vs Spatial Frequency Normalized to the Cut-Off Frequency.	60
28	Modulation Transfer Function for Linear Image Motion . . .	61
29	Waveforms of Image Displacement and Velocity vs Time . . .	61
30	Modulation Transfer Function vs Bar Pattern Spatial Frequency for Sinusoidal Motion of Peak Amplitude of 100, 50, and 25 Microradians per Exposure Time for the Assumed System	63
31	Cut-Off Frequency and the Angular Subtense of Cut-Off Frequency Line Width vs the Peak-to-Peak Angular Amplitude of Sinusoidal Motion	64
32	Modulation Transfer Function for Sinusoidal Motion vs Spatial Frequency Normalized to the Cut-Off Frequency.	65
33	Modulation Transfer Function for Sinusoidal Image Motion	65
34	Modulation Transfer Function for the Assumed System with Random Image Motion of RMS Amplitude 25, 50, and 100 Microradians per Exposure Time	67
35	Cut-Off Spatial Frequency and Angular Subtense of Corresponding Period for the Assumed System as a Function of the RMS Angular Motion per Exposure Time. Angular Subtense is Shown as Solid Line.	68

<u>Figure</u>		<u>Page</u>
36	Modulation Transfer Function vs Spatial Frequency Normalized to the Cut-Off Frequency for Random Image Motion.	69
37	Modulation Transfer Function for Random Image Motion. . . .	69
38	Modulation Transfer Function for Static System and Scene and for System with Scene in Random Motion of RMS Amplitude 50 Microradians with 660 mm Focal Length Lens	70
39	Threshold Resolution vs Input Photocurrent for the Assumed Sensor with a Static Scene and with Random Motion of the Sightline of Magnitude 25 and 40 μrad. $C_M = 0.3$	70
40	Threshold Angular Resolution vs Input Photocurrent for the Assumed Sensor with a Static Scene and with Random Motion of the Sightline of Magnitude 25 and 50 μrad. $C_M = 0.3$	71
41	Threshold Angular Resolution vs Input Photocathode Current Based on the Periodic, Aperiodic and the Average Calculated for the Threshold Resolution in Lines/Pict. Ht. $C_M = 0.1$	72
42	Threshold Angular Resolution vs Input Photocathode with a Random Motion of Amplitude 50 microrad RMS for a WAV and NAV. $C_M = 0.1$	73
43	Ratio of Threshold Angular Resolution in NAV to that in WAV with Random Sightline Motion of Amplitude 50 microrad RMS. $C_M = 0.1$	73
44	Threshold Angular Resolution vs Input Photocurrent Based on the Periodic, Aperiodic and the Average Calculated for Threshold Angular Resolution in Microradians. $C_M = 0.1$	78
45	Corrected Probability of Detection vs SNR_{DI} Required for Rectangular Images of Size $\square 4 \times 4$, $\square 4 \times 64$, $\triangle 4 \times 128$ and $\diamond 4 \times 180$ Lines.	86
46	Threshold SNR_{DI} vs Bar Pattern Spatial Frequency for Display-to-Observer Viewing Distance of $\phi 14''$, $\square 28''$ and $\odot 56''$	87
47	Threshold Video SNR vs Bar Pattern Spatial Frequency for a Video Bandwidth of 10^7 Hz	88

<u>Figure</u>		<u>Page</u>
48	Effect of an Aperture on a Point and Line Source Image	90
49	Schematic of the Input-Output Relationship for an Aperture.	96
50	Illustration of the Effect of an Aperture of Effective Duration $x_0/\alpha = 1.0$ on a Rectangular Input Image in Both the Space and Fourier Domains for $x_0/\alpha = 2.0$	97
51	Fourier Spectra of Unit Amplitude Rectangular Input Pulses of Duration $x_0/\alpha = 8$ and 4. Also shown is the Optical Transfer Function for a Gaussian Impulse Response of Effective Duration $x_0/\alpha = 1.0$	99
52	The Effect of a Gaussian Impulse Response on (-) Unit Amplitude Rectangular Input Pulses of Duration 16, 8, 4, and 1. Output Waveshape is Shown as Dashed Curve. . . .	99
53	Relative Output Pulse Amplitude vs the Width of a Unit Amplitude Rectangular Pulse after Filtering by a Gaussian Aperture of Effective Duration $x_0/\alpha = 1.0$	100
54	Equivalent Output Pulse Width vs the Width of a Unit Amplitude Rectangular Input Pulse of Width x_0/α After Passing Through a Gaussian Aperture of Equivalent Width $x_0/\alpha = 1.0$	101
55	Increase in Noise Perceived by an Observer Due to an Increase in Effective Image Size Due to an MTF Preceding a Point of Noise Insertion	103
56	Signal and Noise Diagram for the Case of an Aperiodic Image with Noise Added Subsequent to an Aperture.	104
57	Normalized Function $F(N)/F(0)$ vs Spatial Frequency and ΔB_N the Noise Equivalent Bandwidth	107
58	(a) Aperture Following a Point of Noise Insertion, and (b) Functional Noise Diagram for (a).	112
59	Apertures Which Both Follow and Precede Points of Noise Insertion	116
60	Schematic of an EBSICON Camera Tube	119
61	Experimental Set Up for Motion Experiments.	122

FigurePage

62	Corrected Probability vs Display Signal-to-Noise Ratio for Target Recognition-Speed 10 Sec/Picture Height; Tank ○ , Truck □ , Derrick ● , Radar Truck ◇ , Televised Images at 875 Lines, 25 Frames/Sec, $D_V/D_H = 3.5$	124
63	Relative Response vs Spatial Frequency for Motion Experiment □ Static Case with Blower on, ○ Pure Motion, 10 Sec/Picture Height for a Frame Time 1/25 Sec.	128
64	Relative Response vs Spatial Frequency--Measured for 10 Sec/Picture Height ■ , Theoretical ●	128
65	Static Amplitude Response for WX 31841.	131
66	Dynamic Amplitude Response for Pattern Speed of 60 Second/Picture Width □ $V_T = 20V$, ■ $V_T = 7.5V$ for WX 31841--Solid Curve Static Case, ● Theoretical.	132
67	Dynamic Amplitude Response for Pattern Speed of 20 Seconds/Picture Width □ $V_T = 20v$, ■ $V_T = 7.5V$ for WX 31841--Solid Curve Static Case, ● Theoretical.	132
68	Dynamic Amplitude Response for Pattern Speed of 10 Seconds/Picture Width □ $V_T = 20V$, ■ $V_T = 7.5V$ for WX 31841--Solid Curve Static Case, ● Theoretical.	133
69	Build Up Lag ● , Decay Lag ○ As a Function of Target Voltage for WX 31911	134
70	Gamma, γ for Different Target Voltages for WX 31911.	134
71	Dynamic Sensitivity for 100% Contrast Pattern, $V_T = 20$ volts ○ static, ● 60 Sec/P.W., □ 20 Sec/P.W., ■ 10 Sec/P.W., ◇ 5 Sec/P.W. Bandwidth 12 MHz.	136
72	Dynamic Sensitivity for 100% Contrast Pattern, $V_T = 7.5$ volts ○ Static, ● 60 Sec/P.W., □ 20 Sec/P.W., ■ 10 Sec/P.W., ◇ 5 Sec/P.W. Bandwidth 12 MHz.	136
73	Dynamic Sensitivity for 35% Contrast Pattern, $V_T = 20$ volts ○ Static, ■ 10 Sec/P.W., Bandwidth 12 MHz.	137
74	Dynamic Sensitivity for 35% Contrast Pattern, $V_T = 7.5$ volts, ○ Static, ■ 10 Sec/P.W., Bandwidth 12 MHz.	137

<u>Figure</u>		<u>Page</u>
75	Experimental Set-Up for the Televised Camera Generated Imagery	140
76	Modulation Transfer Functions for Case A ● , Case B ○ , and Case C □ . Lens and Camera Combined	141
77	Bar Patterns of Variable Aspect, Isolated Bars and Isolated Circles Used for Experiments	142
78	Bar Patterns of Constant Aspect Used for Experiments. . . .	143
79	Exp. No. 1 and 2. Threshold SNR_{DI} for ● Original Data and Present Data ○ Minimum Illumination Back- Ground □ 1 ft-Lambert Background--Constant Aspect Pattern Case A MTF.	148
80	Exp. No. 2 Probability of Bar Pattern Recognition Versus Display Signal-to-Noise Ratio for Case A MTF, 1 ft-Lambert Monitor and 1 ft-Lambert Back- ground Bar Pattern Spatial Frequency ● 104, ● 200, □ 329, ■ 396, ◇ 482, ◆ 635 AF 5 Bar.	148
81	Exp. No. 3 Threshold SNR_{DI} for ● Original Data and Present Data 1 ft.-Lambert Background ○ Normal, □ Very Critical Threshold Judgment--Constant Aspect Pattern Case A MTF.	141
82	The Display Signal-to-Noise Ratio Experiment.	150
83	Exp. No. 4 Threshold SNR_{DI} for Electronically Generated Squares ○ New Data, □ Old Data.	151
84	Exp. No. 5 Probability of Bar Pattern Recognition Constant Aspect Bars--Case B MTF Spatial Frequency ○ 104, ● 200, □ 329, ■ 396, ◇ 482, ◆ 635	153
85	Exp. No. 5 Threshold SNR_{DI} for Constant Aspect Bar Patterns Case B MTF	153
86	Exp. No. 6 Probability of Bar Patterns Recognition for Case C, Constant Aspect Bar Patterns Spatial Frequency ○ 104, ● 200, □ 329	154
87	Exp. No. 6 Threshold SNR_{DI} for Case C, Constant Aspect Patterns	154
88	Threshold SNR_{DI} for AF 5 Bar Pattern Case A ● , Case B ○ , Case C □ MTF's	155

<u>Figure</u>		<u>Page</u>
89	Probability of Bar Patterns Recognition for Constant Length Bar Patterns--Case A MTF.	156
90	Exp. No. 7 Comparison of Threshold SNR_{DI} for Case A MTF, \odot Constant Length, \ominus Constant Aspect Bar Patterns	157
91	Exp. No. 7 and 8 Comparison of Threshold SNR_{DI} for Constant Length Bar Patterns Case A \odot , Case C \square MTF's.	157
92	Exp. No. 9 and 10 Threshold SNR_{DI} for Isolated Bars for Case A \odot , Case C \square MTF's, \diamond Electronically Generated Squares.	158
93	Exp. No. 11 and 12 Threshold SNR_{DI} for Isolated Circles for Case A \odot , Case C \square MTF's, \diamond Electronically Generated Squares	159
94	Photographs of Models Used for Recognition Experiments--Upper Left, Tank; Upper Right, Van Truck; Lower Left, Half Truck with Antenna; and Lower Right, Derrick Half Truck.	160
95	Exp. No. 13 Tactical Target Recognition for Case A MTF \odot Tank, \ominus Derrick, \square Truck, \diamond Radar Truck.	162
96	Exp. No. 14 Tactical Target Recognition for Case C MTF \odot Tank, \ominus Derrick, \square Truck, \diamond Radar Truck.	163
97	Waveform of Derrick Half Truck Along the Horizontal as a Function of Vertical Position of Scan Lines	164
98	Two Modulation Transfer Functions. Curve A Illustrates a High, Low Frequency Response while Curve B Illustrates a High, High Frequency Response.	167
99	MTF, Equivalent Bandwidth N_b and Noise Equivalent Bandwidth, N_e vs Spatial Frequency for a Typical 40/40/25 I-EBSICON Camera Tube	168
100	Output Waveshape (-) for a Step Function Input (---). Shape of Output Waveshape, $\Delta g_i / \Delta x_i$ is used to Find Image Acutance	172
101	Display Signal-to-Noise Ratio Obtainable (-) and Required (---) for Two Light Levels as a Function of Spatial Frequency	176

LIST OF TABLES

<u>Table</u>		<u>Page</u>
1	Levels of Object Discrimination.	21
2	Johnson's Criteria for the Resolution Required per Minimum Object Dimensions vs Discrimination Level.	21
3	Best Estimate of Threshold SNR_{DI} for Detection, Recognition and Identification of Images	25
4	Assumed TV and Scene Parameters.	28
5	Typical Values of the Sky-to-Ground Ratio.	40
6	Values a/A and SNR_V Used for Motion Experiment	124
7	Parameters Used in Calculating SNR_D for Aperiodic Target	126
8	Value of N_{eT} and N_{eL} and Overall N_{eLT} for Three Cases.	141
9	Line Numbers and Bar Aspect for Various Patterns	144
10	Experimental Conditions.	147

1.0 Introduction and Summary

The objectives of the Performance Synthesis Study — Electro-Optical Sensors — performed under Air Force Contract Number F33615-70-C-1461 are to determine the fundamental limitations of long range air-to-ground detection, recognition and identification of tactical military targets, to determine methods of realizing maximum range performance through optimum spatial, temporal and electrical filtering of the received image signals and to devise methods of predicting maximum range performance taking into account the parameters of real targets, backgrounds, illumination sources, atmospheric and sensory systems. The results are to be applicable to all imaging sensors whether passive or active and are to include low-light-level television, forward-looking infrared scanners and direct view light amplifiers.

The current effort is a continuation of the programs previously reported in Ref. 1 (Technical Report AFAL-TR-71-137, May 1971) and Ref. 2 (Technical Report AFAL-TR-72-229). As before, the approach taken is to devise analytical models to describe sensory system performance including the observer as an integral part of the system. Psychophysical experiments are performed to obtain the necessary constants of the observers to quantitatively evaluate the analytical models. Through these efforts, it is hoped to promote a better understanding of the operation of electro-optical sensors, guide the further development of systems components, improve methods of sensory system

performance and reduce the necessity of costly laboratory and flight evaluation of prototype systems.

In the previous efforts reported, the early emphasis in analysis and experimentation was on images of simple or regular geometry such as rectangles and bar patterns. Real images of tactical objects were also considered with a concerted effort to correlate the discernability of bar patterns with various levels of real object discrimination -- particularly real object recognition and identification. Some success with the equivalent bar pattern approach was realized as noted in Ref. 2. However, further efforts were, and still are, required.

The discernability of an image projected onto the photosurface of an electro-optical sensor and ultimately displayed to an observer is limited by the sensor's sensitivity to the received radiation and by noises generated either in the primary photoconversion process or in subsequent signal processing. Also, the image's discernability is limited by finite sensor apertures that decrease the image modulation. Preliminary efforts to account for the effects of these apertures were reported in Ref. 1. The theory, then presented, though leading to reasonable system predictions was intuitively unsatisfying. An advanced theory was presented in Ref. 2 that was more satisfying but still had deficiencies -- particularly in the treatment of aperiodic (rectangular) images.

Concurrent with the effort reported in Ref. 2, a separate effort was undertaken under Air Force Contract Number F33615-70-C-1461 by Sendall and Rosell to analyze FLIR and TV on a common basis. In this program, the aperiodic image treatment was considerably improved due in

large part to Sendall. These advances in the modeling are reported herein in some detail. While much of the ground work for the present models must be attributed to Otto Schade, Sr., the translation of the theory to practice has not proved trivial.

The performance synthesis program as presently constituted is a relatively small program. Specifically, it involves the part time efforts of the authors and the not inconsiderable efforts of many motivated and dedicated Westinghouse engineers who volunteer their efforts in the tedious psychophysical experimentation.

In each of the continuation efforts, there has been an effort to focus on the most critical problems involved in the image discrimination task. In this most recent effort, we have elected to concentrate on the areas of image aperture effects and image motion which are closely allied problems.

In the early days of airborne television, wide fields of view were the rule. Typically, viewfields were $30^{\circ} \times 40^{\circ}$ which are comparable within a factor of 2, to the viewfield of the unaided eye. Scene resolution observed on the display was also comparable to that which could be observed by the unaided eye in the daytime. With passage of time, viewfields have become ever narrower, with fields of view as small or smaller than 1° becoming usual. Under many conditions, the TV augmented observer's resolution of scene detail substantially exceeds that which he can resolve directly. While narrower fields of view have led to longer scene object detection ranges, range cannot be extended indefinitely by simply reducing viewfield. In the more modern systems, the resolution of scene detail is limited not by the lens or TV camera,

but by sightline instability. In TV practice, the effect of sightline instability is to blur the image during the TV image exposure time. These sightline instability effects are analytically considered in some detail in Section 2. Psychophysical experiments using moving images were performed and the results are reported in Section 4. In the psychophysical experimentation, recognition experiments were performed using images moving laterally across the field of view. The primary effect of the motion was to degrade resolution in the horizontal leaving the vertical unchanged (except for some vibration induced in the camera sightline due to the motion apparatus). Efforts were made to model the motion effects. Some apparent success is noted but the efforts must be considered preliminary. Moving image experiments represent a high level of difficulty. In any given experiment, it is difficult to separate the effects of motion interacting with the exposure time from the effects of motion on sensor lag. Also, it is difficult to both define and measure signal levels using complex imagery. However, the initial efforts reported herein are essential to obtain a feel for the magnitude of the problems involved and to form a base for further effort.

To lay the groundwork for the modulation transfer function experiments, we develop the theory of apertures in great detail in Section 3. This includes the latest treatment of the effects of apertures on aperiodic images. In the evolution of the sensor models, aperiodic and periodic images are separately treated. Using these models, it is found that simple aperiodic images can be detected at much longer ranges

than periodic images both in principle and in practice. Preliminary efforts were made to develop a "balanced" resolution concept as discussed in Section 2. The balanced resolution concept is felt to have merit when based on the average angular scene resolution (rather than the average limiting resolution based on threshold spatial frequency). The preferred averaging technique weights the periodic model more heavily which is felt to be in the right direction.

The detailed theory of apertures developed in Section 3 is used to update the model of Section 2 and, as we noted, to serve as a foundation for the MTF related psychophysical experimentation having to do with both image motion and fixed sensor apertures. The theory of the effect of apertures is well developed and mathematically rigorous. However, the observer is an integral part of the system and the mathematical rigor must therefore include the human element and thus the theory must be confirmed through psychophysical experiments. To our knowledge, experiments to confirm the theory have not been performed except to show first order effects.

The psychophysical experimentation reported in Section 5 is devoted to modulation transfer function effects. Different MTF characteristics were obtained by defocusing of the cameras objective lens. Specified in terms of Schade's noise equivalent passband, N_e , the best MTF had an N_e of 252 and the poorest had an N_e of 69. The experiments made with constant aspect and constant length bar patterns appear to indicate that the current theory yields results that are somewhat pessimistic for MTF's with low N_e (poor MTF). Experiments with isolated bars and circles indicate that the theory

correctly accounts for the MTF effects. Using images of real objects (vehicles), it was found that the results predicted on the basis of theory are again pessimistic but to a lesser extent than that predicted for the periodic patterns. The periodic theory of apertures thus appears to need further work.

For many years, researchers in the optical field have sought a single unit figure of merit for sensory systems. Whether such a unit has much in the way of practical merit is open to debate but in the quest, a better understanding of the parameters that determine image quality should evolve. In Section 6, a number of the figures of merit previously proposed are reviewed. Most of the figures of merit involve some integral of the modulation transfer function or equivalently, the integral of the point spread function. A primary difference between various measures is the weight applied to the functions before integrating.

Most of the figures of merit do not include sensitivity or signal-to-noise as a parameter. Thus a sensor with a very high figure of merit may be far inferior to one with a low figure in a given application. For example, a very high resolution vidicon would be inferior to a low resolution LLLTV when a night scene is to be viewed. When signal-to-noise ratio is included as a parameter, the figure of merit usually ceases to be a single number but rather, becomes a function. In recent work, attempts have been made to include sensitivity and noise in the figure of merit. The concept is to integrate the area between the signal curve and the noise curve (with signals and noises expressed as a function of spatial frequency). The principal deficiency of

this scheme is the problem of selecting the low frequency limit.

It is clear that finding a single figure of merit for a sensory system is highly unlikely. The figure of merit will undoubtedly be a function and will include both sensitivity and resolution parameters. The threshold resolution vs photosurface irradiance characteristic of a sensor, used extensively by television designers, is a figure-of-merit function based on bar pattern inputs. This characteristic includes the sensor sensitivity, MTF and noise parameters but the characteristic may not be in the most useful form and it has not been related to a picture quality criterion. A figure of merit based on the threshold resolution characteristic has been proposed by Schade and will be discussed in the follow-on efforts.

2.0 Range Analysis and Model Update

In this section, we shall review the efforts made during the current program to improve the analytical electro-optical-sensor-augmented observer model and show the practical application of the model to imaging systems. In Section 2.1, the sensor model and observer requirements, as previously reported in Refs. 1 and 2 and updated in this report, are discussed. The model is applied to a passive electro-optical imaging system in Section 2.2 and to an active electro-optical imaging system in Section 2.3. In these sections, the scene is assumed to be stationary relative to the sensor. In Section 2.4, the effects of relative image motion on overall system performance will be taken into account to the extent that these effects are now understood. In all of these analyses, the emphasis is in determining the range at which specific scene objects can be detected, recognized and identified under varying scene and atmospheric conditions. In Section 2.5, a balanced resolution concept is discussed.

2.1 The Sensor Model and Observer Requirements

The analysis and experimentation discussed in this report and the two which preceded it are based on the concept that signal-to-noise ratio can be associated with a scene object after it has been imaged by a lens and phototransduced by a photosensitive surface. The image is then further processed by the electro-optical system. In this processing, signal-to-noise ratio is lost. Knowing the system parameters, the amount lost can be readily calculated for images of simple or regular geometric shape.

Eventually, the sensor recreates a visible light image on a display which may be directly viewed by an observer. With good design, the electro-optical sensor displays the image with sufficient size and luminance to insure that the observer will not be acuity or light-level limited. If this is the case, the system determines the image signal-to-noise ratio and not the observer's eye except that, due account must be taken of the ability of the observer to integrate over the area of the image and to integrate over a period of time.

In the elementary sensory system model reviewed in Section 3.1, it is assumed that the displayed image is signal limited by the image's size and irradiance level and further limited by noises generated either in the scene photon-to-sensor-photoelectron conversion process or by the system itself. Then, it is shown that the image's discernability can be further reduced by the sensor's finite apertures. By finite apertures, we mean those elements or processes in the sensor which cause a blurring of the image. In an ideal sensor, a point object would be imaged as a point on the display. In a real system, the lens causes the point to become a blur circle in the image plane due to diffraction, lack of focus and aberration effects. The image may then be further blurred by fiber-optic faceplates, electron lens defects, phosphor particles, lateral spread in charge storage targets and the finite diameters of electron beams. Some blurring effects are intentionally introduced. For example, the horizontal resolution in a TV camera may be video bandwidth limited and the display beam may be intentionally defocused in the vertical to minimize the raster structure. These blurring effects on the image are quantitatively described in terms of the optical transfer functions of individual

system elements and are taken into account in analyzing the image signal-to-noise ratios.

The observer is an integral part of a real time imaging system and the system's overall performance must take the observer's requirements into account. For simplicity, we divide the total imaging problem into three parts which are: the properties of the scene, the capability of the imaging system and the requirements of the observers. The ability of the observer to resolve imaged scene detail is determined by matching the signal-to-noise ratio of an image appearing on the output of the electro-optical sensor's display to that required by the observer to discern the image at a given level of detail.

The properties of the scene will be discussed in the next two sections. In this section, we will concentrate on the sensor and observer requirements. We note first that the lens images the scene on the input photosurface which converts the scene photons to photoelectrons. The rate at which the photoelectrons are generated can be described in terms of a current, i . In the development of the elementary model, it was found that the signal-to-noise ratio of an image appearing on the display of a typical television camera could be written as

$$SNR_D = \left[\frac{t}{\alpha} \left(\frac{a}{A} \right) \right]^{\frac{1}{2}} \frac{2C_M G i_{av}}{[eG^2 i_{av} + I_p^2 / 2\Delta f_V]^{\frac{1}{2}}} \quad (1)$$

where t is the integration time of the observer's eye, a is the image area, α is the picture aspect ratio (W:H), A is the total effective

photosurface area, C_M^* is the image modulation contrast, G is the pre-storage gain of the TV camera tubes gain storage target, i_{av} is the average photocurrent, e is the charge of an electron, I_p^2 is the mean square system (preamplifier) noise added subsequent to the readout of the image by the electron beam and Δf_V is the video bandwidth. In deriving the above equation, it was assumed that the image area, a , is large relative to the overall system blur circle, that the photoelectron image is amplified by an amount, G , before being stored and read out, and that the only sources of noise are the photoelectron noise and the preamp noise, both of which are white in character. When the above conditions prevail, the above equation applies equally well to the detection of simple geometric shapes such as squares or rectangles and to bar patterns. For squares or rectangles, a is the area of the square or rectangle while for bar patterns, a is the area of a single bar. The areas, a , have some restrictions but these restrictions can generally be neglected for the usual class of imaging tasks.

Simple rectangular objects against a uniform background are designated as aperiodic objects while a bar pattern is designated as a periodic object in the direction transverse to the bars. Whether periodic or aperiodic, it is often an analytical convenience to describe the dimensions of the object's image in terms of dimensionless reciprocals, i.e., if the image dimensions are Δx by Δy and if the image plane height is Y , then we define

$$* C_M = (i_{\max} - i_{\min}) / (i_{\max} + i_{\min}).$$

$$N = \frac{Y}{\Delta x} \frac{\text{lines}}{\text{picture height}} , \quad (2)$$

$$N_Y = \frac{Y}{\Delta y} = \frac{Y}{\epsilon \Delta x} = \frac{N}{\epsilon} , \quad (3)$$

where ϵ is equal to the ratio $\Delta y / \Delta x$. The quantity N , when used to describe a bar pattern has the form of a spatial frequency which is a convenience when performing Fourier analysis of the image in the frequency domain. With Eqs. (2 and 3), Eq. (1) becomes

$$\text{SNR}_D = \left[\frac{t \epsilon}{\alpha} \right]^{\frac{1}{2}} \frac{1}{N} \frac{2 C_M C_i \text{av}}{[e G^2 i_{\text{av}} + I_p^2 / 2 \Delta f_V]^{\frac{1}{2}}} . \quad (4)$$

In the above, the image is a function of x and y . In the following, we will assume that the x and y variables of the image, and of the apertures which blur the image are independent and separable so that the images can be independently analyzed in the x and y directions.

Suppose that the imaging system has two principal apertures, the lens and the camera tube's gain storage target. Let the modulus of the lens' optical transfer function be $|R_{OL}(N)|$ and that of the target be $|R_{OT}(N)|$. The quantities $|R_{OL}(N)|$ and $|R_{OT}(N)|$ are known as the modulation transfer functions or MTFs. The lens MTF precedes the point of photoelectron noise insertion (at the photosurface) while the target follows the point of photoelectron noise insertion but precedes the point of preamplifier noise insertion as shown in Fig. 1.

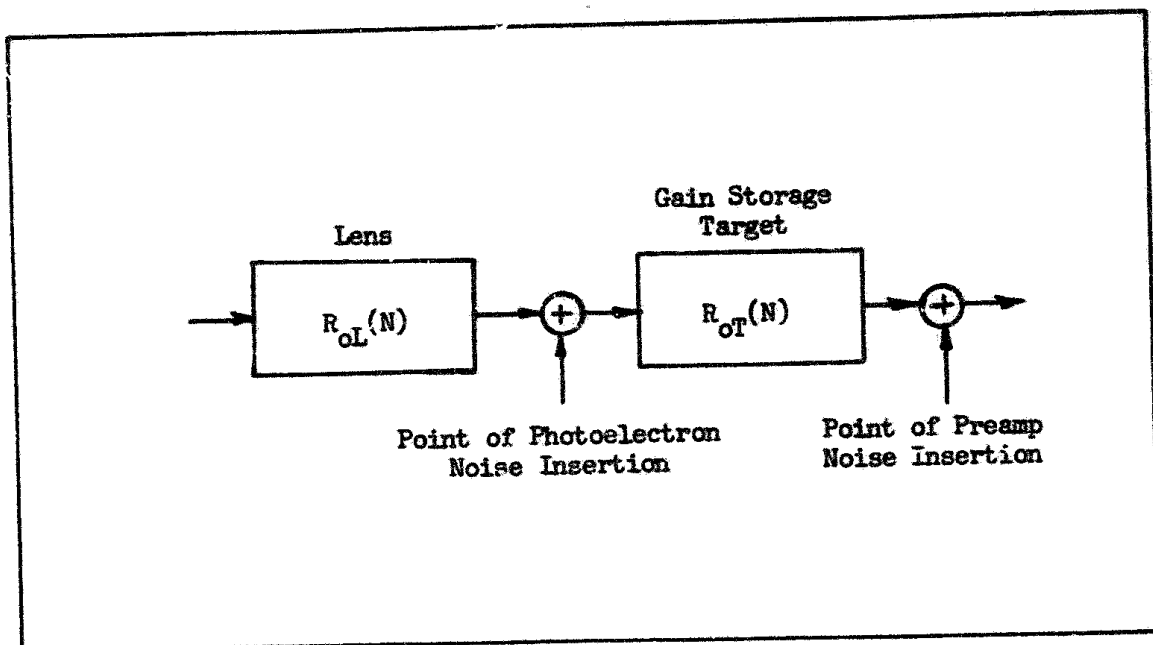


Fig. 1 Location of Points of Noise Insertion Relative to the MTFs.

If the input image is aperiodic, both the lens and target MTFs will increase the noise perceived by the observer. However, the magnitude of the increase depends upon the location of the MTF relative to the point of noise insertion. The lens increases the photoelectron and the preamp noises by the same factor since it precedes both noise insertion points. However, the target filters or bandlimits the photoelectron noise since it follows its point of noise insertion. Thus, the target MTF has a relatively greater effect on the preamp noise than on the photoelectron noise.

The noise increase factor for aperiodic images is given approximately by

$$\xi_{xLT} \cdot \xi_{yLT} = \left[1 + \left(\frac{\delta_L}{\Delta x_i} \right)^2 + \left(\frac{\delta_T}{\Delta x_i} \right)^2 \right]^{\frac{1}{2}} \cdot \left[1 + \left(\frac{\delta_L}{\Delta y_i} \right)^2 + \left(\frac{\delta_T}{\Delta y_i} \right)^2 \right]^{\frac{1}{2}}, \quad (5)$$

where Δx_1 and Δy_1 are in units of picture heights and, δ_L and δ_T are the noise equivalent apertures defined by the equations

$$\delta_L = \frac{1}{N_{eL}} = \frac{1}{\int_0^\infty |R_{oL}(N)|^2 dN} \quad (6)$$

$$\delta_T = \frac{1}{N_{eT}} = \frac{1}{\int_0^\infty |R_{oT}(N)|^2 dN} \quad (7)$$

Note that by Eqs. (2, 3, 6 and 7), Eq. (5) may be written in the equivalent form

$$\xi_{xLT} \cdot \xi_{yLT} = \left[1 + \left(\frac{N}{N_{eL}} \right)^2 + \left(\frac{N}{N_{eT}} \right)^2 \right]^{\frac{1}{2}} \cdot \left[1 + \left(\frac{N}{N_{eL}} \right)^2 + \left(\frac{N}{N_{eT}} \right)^2 \right]^{\frac{1}{2}} \quad (8)$$

In the above, it is assumed that the sensor MTF is the same in both the x and y directions. The filtering effect of the target on the photoelectron noise is given by

$$\Gamma_{xT} \cdot \Gamma_{yT} = \frac{\xi_{xLT} \cdot \xi_{yLT}}{\left[1 + \left(\frac{\delta_L}{\Delta x} \right)^2 + 2 \left(\frac{\delta_T}{\Delta x} \right)^2 \right]^{\frac{1}{2}} \cdot \left[1 + \left(\frac{\delta_L}{\Delta y} \right)^2 + 2 \left(\frac{\delta_T}{\Delta y} \right)^2 \right]^{\frac{1}{2}}} \quad (9)$$

or equivalently,

$$\Gamma_{xT} \cdot \Gamma_{yT} = \frac{\xi_{xLT} \cdot \xi_{yLT}}{\left[1 + \left(\frac{N}{N_{eL}} \right)^2 + 2 \left(\frac{N}{N_{eT}} \right)^2 \right]^{\frac{1}{2}} \cdot \left[1 + \left(\frac{N}{N_{eL}} \right)^2 + 2 \left(\frac{N}{N_{eT}} \right)^2 \right]^{\frac{1}{2}}} \quad (10)$$

These results are incorporated into the Eq. (4), as follows

$$\text{SNR}_D = \left[\frac{t_s}{\alpha} \right]^2 \cdot \frac{1}{(\xi_{xLT} \cdot \xi_{yLT})^2 N} \frac{2C_M G_T i_{av}}{\left[G_T^2 e \Gamma_{xT} \Gamma_{yT} i_{av} + \frac{I_p^2}{2\Delta f_V} \right]^2} \quad (11)$$

As we discussed above, the noise increase factors affect the photoelectron noise and the preamp noise equally but the target exerts a filtering action on the photoelectron noise. We note, however, that the target increases the perceived photoelectron noise more than it filters it.

A bar pattern is periodic in one direction and aperiodic in the other. Assume that the bar pattern is periodic in the x direction. In the periodic x direction, the primary effect of the lens and target will be to decrease the signal modulation and leave noise unchanged. However, as before, the target will exert a filtering effect on the photoelectron noise. The decrease in signal modulation is given by the square wave flux factor, $R_{SF}(N)$. The square wave flux factor is related to the overall system MTF, $|R_{OS}(N)|$, by the formula,

$$R_{SF}(N) = \frac{8}{\pi^2} \sum \frac{|R_{OS}(kN)|}{k^2}, \quad \text{for } k \text{ odd.} \quad (12)$$

The purpose of this calculation is to convert the signal waveform to a mean signal, i.e., SNR_D is proportional to the mean signal-to-rms noise ratio not the peak-to-peak or rms signal.

The targets filtering action on the photoelectron noise in the

periodic direction is given by

$$\beta_{xT} = \int_0^N \frac{|R_{ST}(N)|^2}{N} dN . \quad (13)$$

Using Eqs. (12 and 13) in Eq. (4), we obtain

$$SNR_D = \left[\frac{t\epsilon}{\alpha} \right]^{\frac{1}{2}} \frac{R_{SF}(N)}{(\xi_{yLT})^{\frac{1}{2}N}} \frac{2C_M G_T i_{av}}{[G_T^2 e \Gamma_{yT} \beta_{xT} i_{av} + I_p^2 / 2\Delta f_V]^{\frac{1}{2}}} . \quad (14)$$

In the above, we have observed that the image is aperiodic in the y direction so that the noise increase factor is

$$\xi_{yLT} = \left[1 + \left(\frac{N}{\epsilon N_{eL}} \right)^2 + \left(\frac{N}{\epsilon N_{eT}} \right)^2 \right]^{\frac{1}{2}} , \quad (15)$$

and the noise filtering factor is

$$\Gamma_{yT} = \frac{\xi_{yLT}}{\left[1 + \left(\frac{N}{\epsilon N_{eL}} \right)^2 + 2 \left(\frac{N}{\epsilon N_{eT}} \right)^2 \right]^{\frac{1}{2}}} , \quad (16)$$

for the y direction. Ordinarily, the bars in the pattern are quite long ($\epsilon \gg 1$) relative to their spacing so that the noise increase and filtering factors in the y direction can be neglected (but not always).

The Eqs. (11 and 14) are used to determine the image signal-to-noise ratio obtainable from the sensor for images of simple or regular geometry. In the previous effort (Ref. 2), it was postulated that the detectability of these simple geometric images could be correlated with the detectability, recognizability and identifiability of real images by suitably selecting an equivalent simple image.

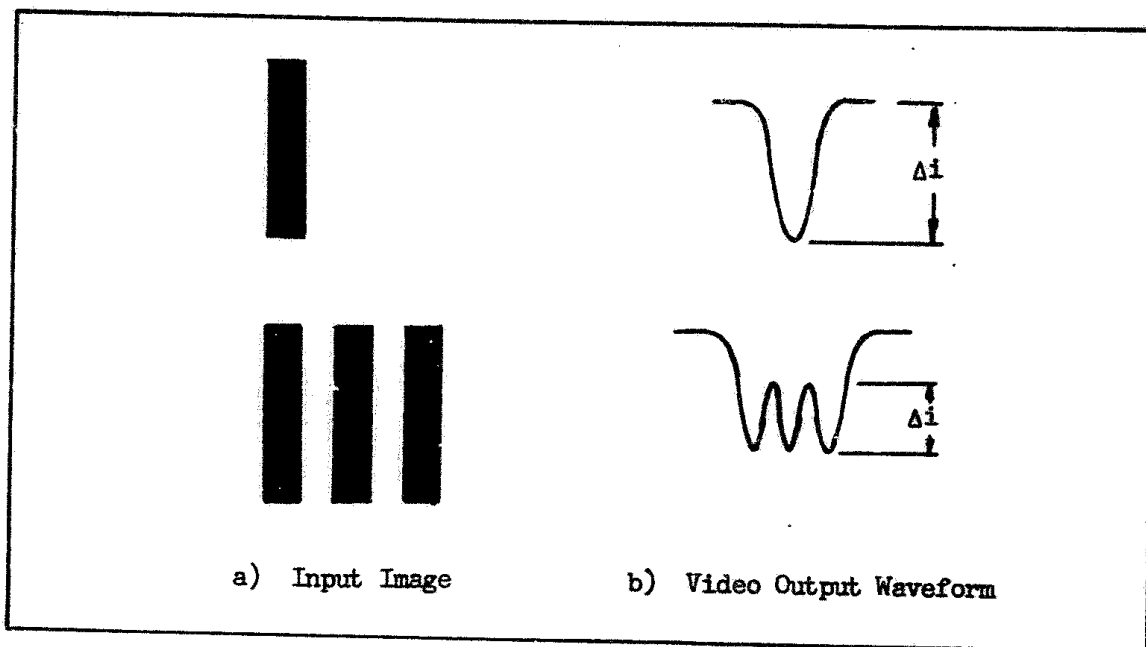


Fig. 2 Video Output Waveforms for a Single Isolated Bar and a Repetitive Bar Pattern.

In Fig. 2a, an isolated single bar is shown along with a bar pattern. The width of the single bar is equal to the width of the bars or spaces in the bar pattern. The expected waveform of the images traverse to their width is shown as they might appear in the video channel in Fig. 2b. Although the irradiance level of the single bar is the same as for the bar pattern, the incremental signal, Δi , is larger for the single bar than for bars within the bar pattern due to the sensor's modulation transfer function. We have postulated in the past, that an observer, in detecting the presence of a bar pattern, must detect the presence of a single bar in the bar pattern. We have found that this postulate is reasonable and that the signal-to-noise ratio needed by the observer to detect the presence of an isolated bar is approximately the same as the signal-to-noise ratio needed to detect the bar in the bar pattern.

However, as was illustrated in Fig. 2, the signal obtainable from the sensor is larger for the isolated bar than it was for the bar in the bar pattern.

Thus, the SNR_D as calculated using aperiodic objects using Eq. (11) can be expected to be larger than the SNR_D using Eq. (14). This will be of consequence as we attempt to correlate the detectability of real scene object with the detectability of simple geometric test objects.

A real scene hardly ever consists of periodic or isolated aperiodic objects. An example of an isolated aperiodic object is an aircraft imaged against a clear sky background. A recently plowed or cultivated field might qualify as a periodic scene object. When the object qualifies as an isolated aperiodic object, the Eq. (11) is directly applicable and similarly the Eq. (14) qualifies when the scene is periodic. In general, specific scene objects are neither periodic or aperiodic (in the sense that we are using aperiodic) but somewhere in between. In the foregoing paragraph, we observed that SNR_D calculated on the basis of an aperiodic object will be larger than the SNR_D calculated for a periodic object. In turn, we will see that system "resolution" will be higher for the aperiodic object than for the periodic object when resolution is specified in terms of the smallest bar width that can be discerned.

In the previous effort (Ref. 2), it was proposed that levels of object discrimination, i.e., detection, orientation, recognition and identification be established along the lines suggested by Johnson (Ref. 3). In this scheme, a scene object is replaced by an equivalent bar pattern. The bar pattern was to be constructed with bar length equal to the length of the object and with bar widths equal to the object's minimum

dimension divided by a factor k_d . The factor k_d is small for low levels of object discrimination such as simple detection or orientation and larger for high levels of discrimination such as recognition or identification. The definitions of the levels of discrimination are given in Table 1 and the discrimination factors, k_d , are tabulated in Table 2. The principal discrimination levels are detection, recognition and identification. The equivalent bar patterns corresponding to these discrimination levels are illustrated schematically in Fig. 3 and the geometric relations from a systems viewpoint for the identification case are illustrated in Fig. 4.

We note that the replacement of an object by an equivalent bar pattern for the detection case involves substantial changes in the detection concept. For an aperiodic object, the SNR_D is based on the total area of the object's image. With the equivalent bar pattern notion, the SNR_D is calculated on the basis of $1/2$ the area. Secondly, for an aperiodic object, the SNR_D is calculated using Eq. (11) while with the equivalent bar pattern approach, SNR_D is calculated using Eq. (14). Again, we note that even for objects of the same image area, SNR_D calculated on the basis of Eq. (11) will be higher than SNR_D calculated on the basis of Eq. (14). On the other hand, the isolated aperiodic case, while it does occur, is unrealistic when used to predict the detectability of the usual terrestrial object amid a low to moderately cluttered background. When objects in severe clutter are to be detected; resolution calculated even on the basis of Eq. (14) for the periodic pattern may be too high. For some situations, it may be necessary to recognize an object to detect it.

<u>Classification of Discrimination Level</u>	<u>Meaning</u>
Detection	An object is present.
Orientation	The object is approximately symmetrical or unsymmetrical and its orientation may be discerned.
Recognition	The class to which the object belongs may be discerned (e.g., house, truck, man, etc.).
Identification	The target can be described to the limit of the observer's knowledge (e.g., motel, pick-up truck, policeman, etc.).

Table 1 Levels of Object Discrimination.

<u>Discrimination Level</u>	<u>Discrimination Factor, k_d, in terms of the Number of Resolution Lines Required per Minimum Object Dimension (TV Lines)</u>
Detection	2.0 ± 1.0 $- 0.5$
Orientation	2.8 ± 0.8 $- 0.4$
Recognition	8.0 ± 1.6 $- 0.4$
Identification	12.8 ± 3.2 $- 2.8$

Table 2 Johnson's Criteria for the Resolution Required per Minimum Object Dimension vs Discrimination Level.

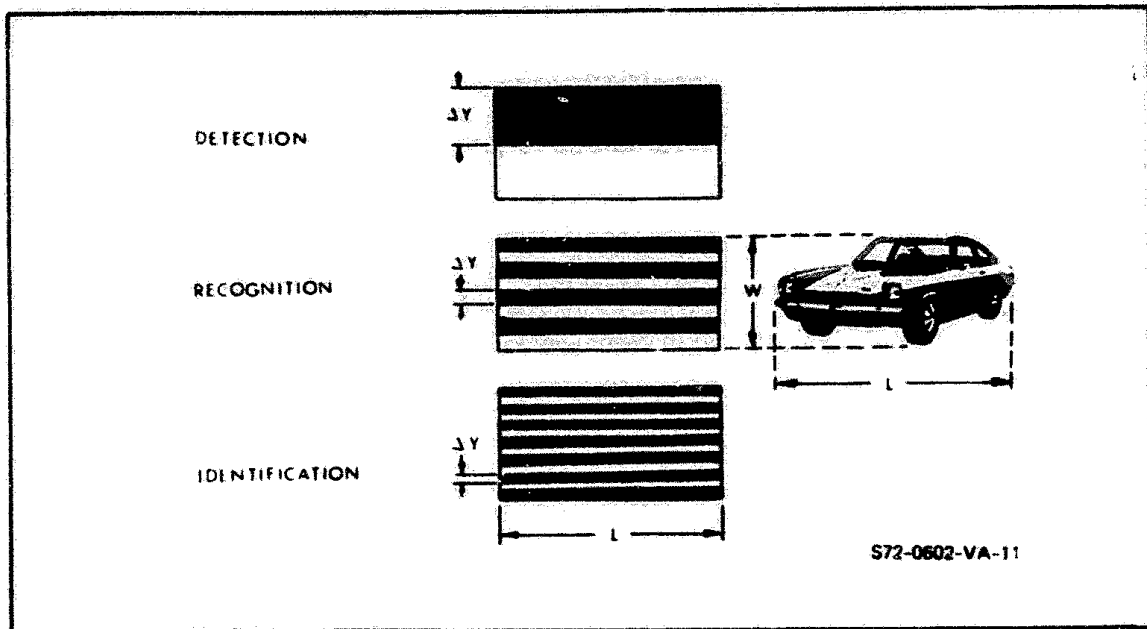


Fig. 3 Levels of Object Discrimination. Object Area to be Used in the SNR_D Calculation is ΔY by L .

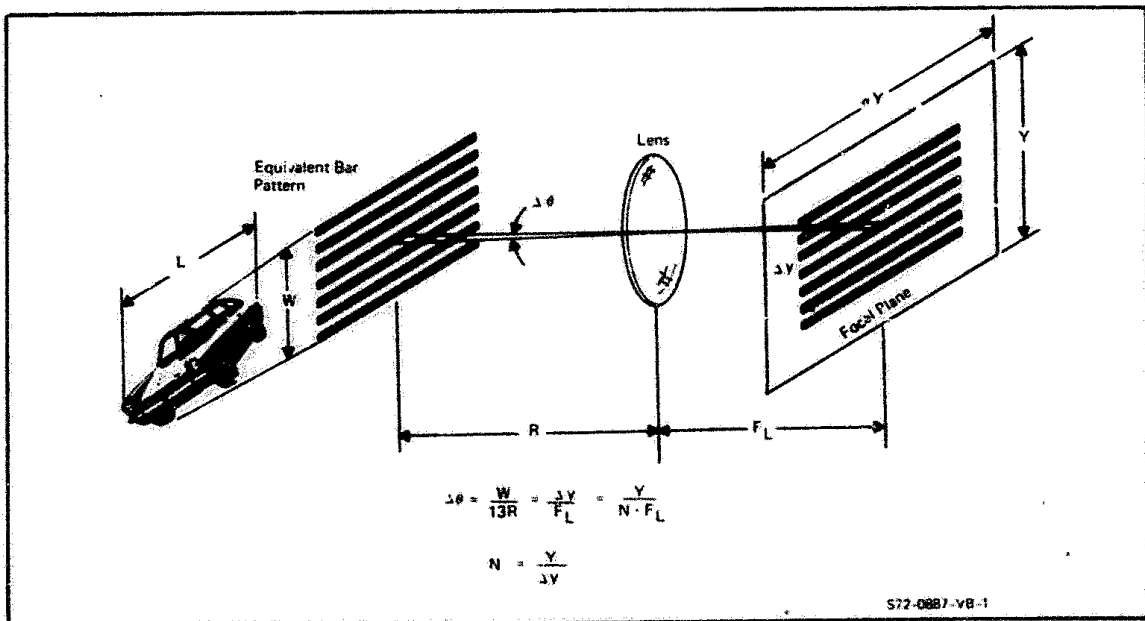


Fig. 4 Equivalent Bar Pattern Criterion for Object Identification.

For the recognition case, we face a dilemma similar to the detection case. To recognize an object, it is probable that the objects outline must be discerned with a fairly high degree of clarity. However, the outline is by no means periodic but the prediction of an object's recognizability and identifiability of real scene objects, such as vehicles were correlated with the detectability of an equivalent bar pattern. The correlation, based on the threshold SNR_D required by the observer appeared surprisingly good and perhaps too good because of a difference in the method of calculating signal as we noted at the time. In the case of the real object, we calculated the threshold signal-to-noise ratio on the basis of the peak signal excursion above (or below) background while for the equivalent bar pattern, we used the signal excursion within the bar pattern structure as noted in Fig. 2b. Had we calculated SNR_D for the real object on the basis of the mean signal excursion rather than the peak signal above background, the SNR_D at threshold would have been smaller for the real object.

When the visual task is to detect a truly aperiodic object, such a water tower against the horizon sky, the analysis is clear cut, as noted before. The aperiodic Eq. (11) is used. For more complex scenes or levels of discrimination we suggested in Ref. 2, as a possible compromise, a dual resolution criterion wherein the resolution is first calculated on the basis of an aperiodic object and then on the basis of a periodic object. The overall system resolution is then estimated to be the arithmetic average of the periodic and aperiodic object resolution. It is tentatively proposed that the total object areas are to be chosen in the following manner. Suppose the equivalent scene object

is a rectangle of area equal to the area of the real object, of width approximately equal to the object's minimum dimension and of length approximately equal to the area of the real object's area divided by its width.

However, the SNR_D , and in turn, the resolution, is calculated for an area equal to the width of the equivalent area divided by the discrimination factor of Table 2. For detection, in a moderately cluttered area, the object area, for purposes of calculation, is the equivalent object width divided by 2, times the equivalent object length. This is true for both the periodic and aperiodic image calculation when the dual criterion is used. Similarly, for recognition, the object area for calculation purposes, is the equivalent object width divided by 8, times the equivalent object length.

In calculating resolution, we match the image signal-to-noise ratio obtainable from the sensor to that required by the observer. This usually involves a trial and error or a graphical solution to determine scene object resolution thresholds. A somewhat simpler approach might be to average the SNR_D 's calculated on the periodic/aperiodic bases and calculate resolution thresholds on the average. This could be a good approximation.

The detection of simple aperiodic objects such as squares and rectangles can be precisely predicted. Similarly, we can predict the detectability of periodic bar or sine wave patterns with high accuracy. It can, however, be correctly inferred that the extension of the theory of detection of simple periodic or aperiodic objects to real scene objects is an unprecise art needing considerable further work.

Discrimination Level	Background	k_d TV Lines per Minimum Dimension	Threshold SNR_{DI} for Spatial Frequency (Lines/Pict. Ht.) of			
			100	300	500	700
Detection	Uniform*	1	2.8	2.8	2.8	2.8
Detection	Clutter	2	4.8	2.9	2.5	2.5
Recognition	Uniform	8	4.8	2.9	2.5	2.5
Recognition	Clutter	8	6.4	3.9	3.4	3.4
Identification	Uniform	13	5.8	3.6	3.0	3.0

* Treated as an Aperiodic Object.

Table 3 Best Estimate of Threshold SNR_{DI} for Detection, Recognition and Identification of Images.

Fortunately, the sensitivity of the equations to the various alternative criteria, when real scene parameters are taken into account, is not large so that reasonable predictions result.

We observed that to obtain resolution predictions, it is necessary to determine observer signal-to-noise ratio requirements. A large number of psychophysical experiments were performed to determine these observer requirements for various visual tasks and were reported in Ref. 2. Further work in this area has been undertaken and is reported in this document. In Ref. 2, the threshold signal-to-noise ratios required by the observer for various levels of object discrimination were experimentally determined using the equivalent bar pattern approach and are noted in Table 3. We note once again that the threshold signal-to-noise ratio values indicated were based on the equivalent bar pattern approach and apply to

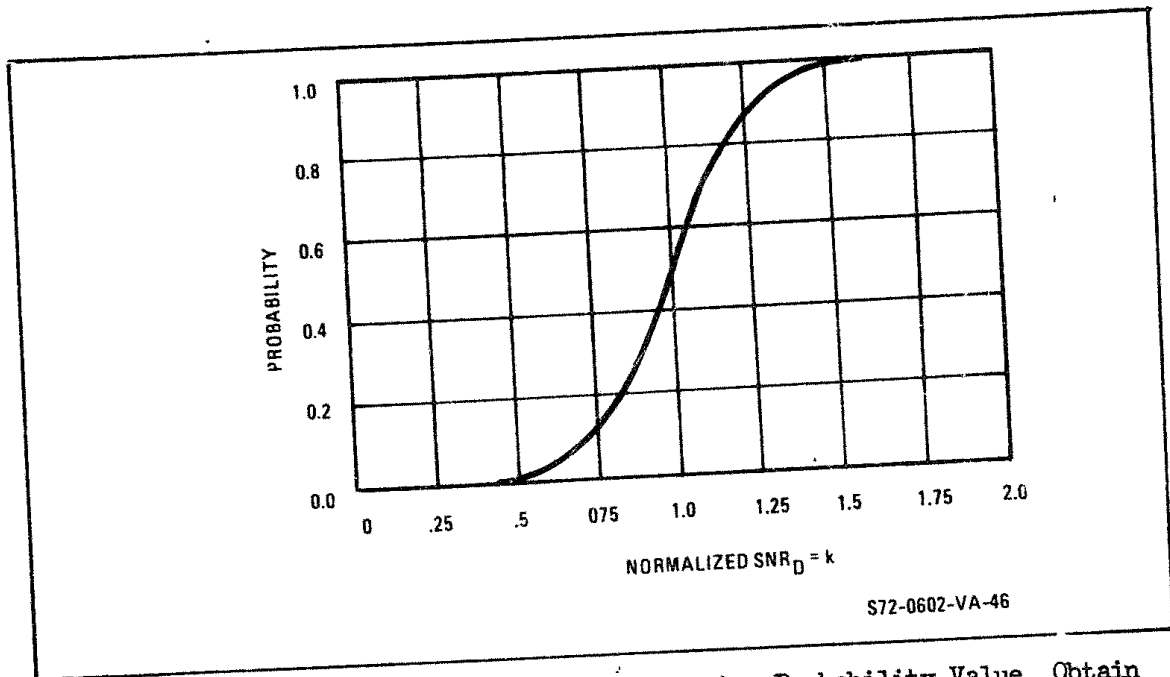


Fig. 5 Probability vs Normalized SNR_{DI} . For Any Probability Value, Obtain SNR_{DI} from Table 3 for 50% Probability. Find Value of k for Desired Probability and Multiply Value of SNR_{DI} by k to Obtain New Value of SNR_{DI} Required.

a fixed observer viewing distance to displayed picture height ratio of 3.5:1 which penalizes the detection of low frequency bar patterns. We also noted in Ref. 2 that the signal-to-noise ratio calculated for the recognition and identification of real objects was performed in a somewhat different manner than for the equivalent bar pattern with the probable result that the SNR_D values of Table 3 are too high. This inequity will be compensated in part by use of the dual periodic-aperiodic image calculation approach.

Again, we note that the resolution prediction equations are not of great sensitivity to the signal-to-noise ratio thresholds. For first cut calculations, we shall assume that the observer requires a signal-to-noise ratio of 3.0 to detect either an aperiodic or periodic object at the 50% level of probability and, that this number is

relatively independent of the equivalent bar pattern's spatial frequency. For other values of probability, the threshold signal-to-noise ratio should be increased by the factor shown in Fig. 5.

With the understandings developed above, we progress to examples of range prediction starting first with the passive scene imaging case followed by the active image case. Initially, we will consider the relative scene camera motion to be zero and then discuss motion as a factor.

2.2 Passive Television Imaging System

A passive imaging system is one which images a scene lighted only by natural scene sources such as the sun, moon, sky or stars. To illustrate the analysis of a passive system, we will consider a specific television telescope with parameters as given in Table 4. This system is primarily intended for daylight use but twilight capability is desired. The level of object discrimination required is the recognition of scene objects which are of essentially square geometry. We will first assume that the scene is stationary and that no atmosphere intervenes between the scene and observer. Then the case of restricted visibility will be considered and later, in Section 2.4, we will consider relative sensor-to-scene motion.

The TV systems MTF and MTF related parameters are given in Table 4 and Fig. 6. The principal MTFs are those of the lens and the camera tube target. Using Eq. (14), the SNR_D is calculated for the periodic equivalent bar pattern and plotted in Fig. 7. Similarly, the SNR_D is calculated using the aperiodic Eq. (11) and are plotted in Fig. 8.

LENS

Field-of-View	$1.13^{\circ} \times 0.85^{\circ}$
Focal Length	660 mm
T/Stop	10
MTF	Fig. 10
Noise Equiv. Bandwidth (N_e)	330 Lines/Pict. Ht.

CAMERA TUBE

Type	16/16 mm EBSICON
Photocathode	
Type	S-25
Responsivity	3.2 mA/W (2854° K Source)
Effective Area	$1.28 \times 10^{-4} \text{ m}^2$
Gain-Storage Target	
Type	Silicon Diode Matrix
Diameter	16 mm
Gain	2 to 2000 (Variable)
Max Average Signal Current	3×10^{-7} Amperes
MTF	Fig. 10
Noise Equiv. Bandwidth	170 Lines/Pict. Ht.

VIDEO PROCESSOR

Preamplifier Noise	6×10^{-9} Ampere
Video Bandwidth	6×10^6 Hz

SCENE

Object Geometry	Square
Level of Discrimination	Recognition
Equivalent Bar Ht. to Width Ratio (e)	8
Irradiance	Variable
Average Reflectivity	0.15

Table 4. Assumed TV and Scene Parameters.

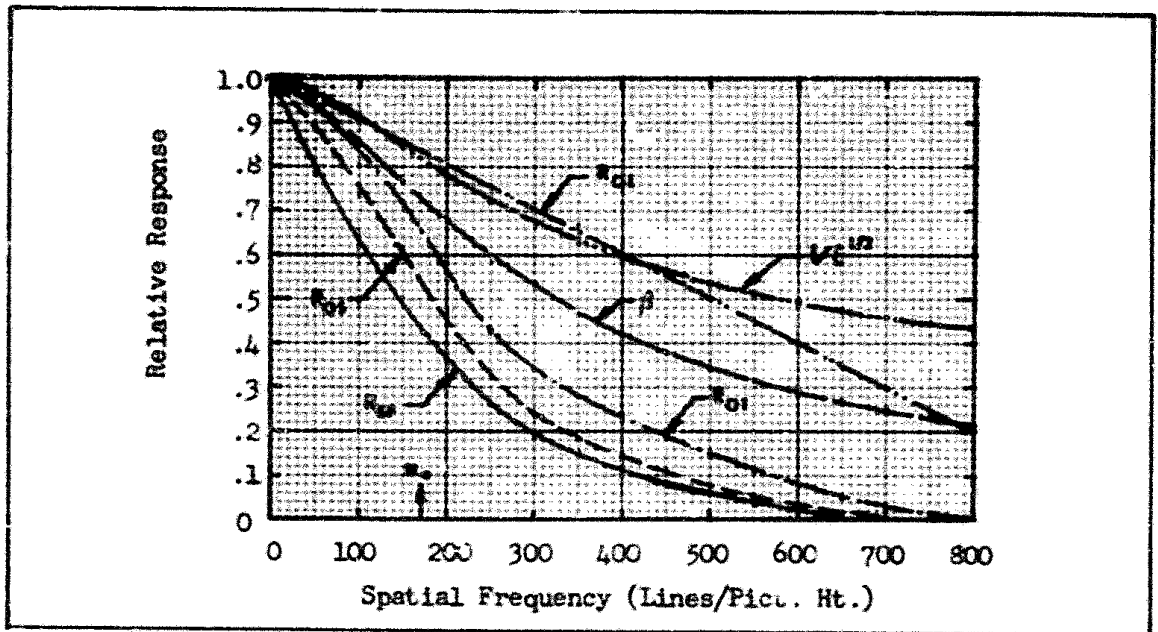


Fig. 6 MTF and MTF Related Functions for the Assumed Sample System.

These curves represent the image signal-to-noise ratio obtainable from the sensor. On the same curves, we show the observer's signal-to-noise ratio thresholds. The observer's threshold SNR_{DT} , as we noted in the previous section is approximately constant and independent of the input image contrast. As scene object contrast is reduced, the SNR_D obtainable from the sensor decreases. However, for analytical convenience, it is assumed that the observer's SNR_{DT} increases as the object contrast decreases, i.e.,

$$SNR_{DT} \text{ (for Object Contrast, } C_M) = \frac{SNR_{DT} \text{ (for } C_M = 1.0)}{C_M}. \quad (17)$$

This assumption greatly reduces the number of curves to be drawn.

The intersection of the SNR_D and SNR_{DT} curves gives the threshold

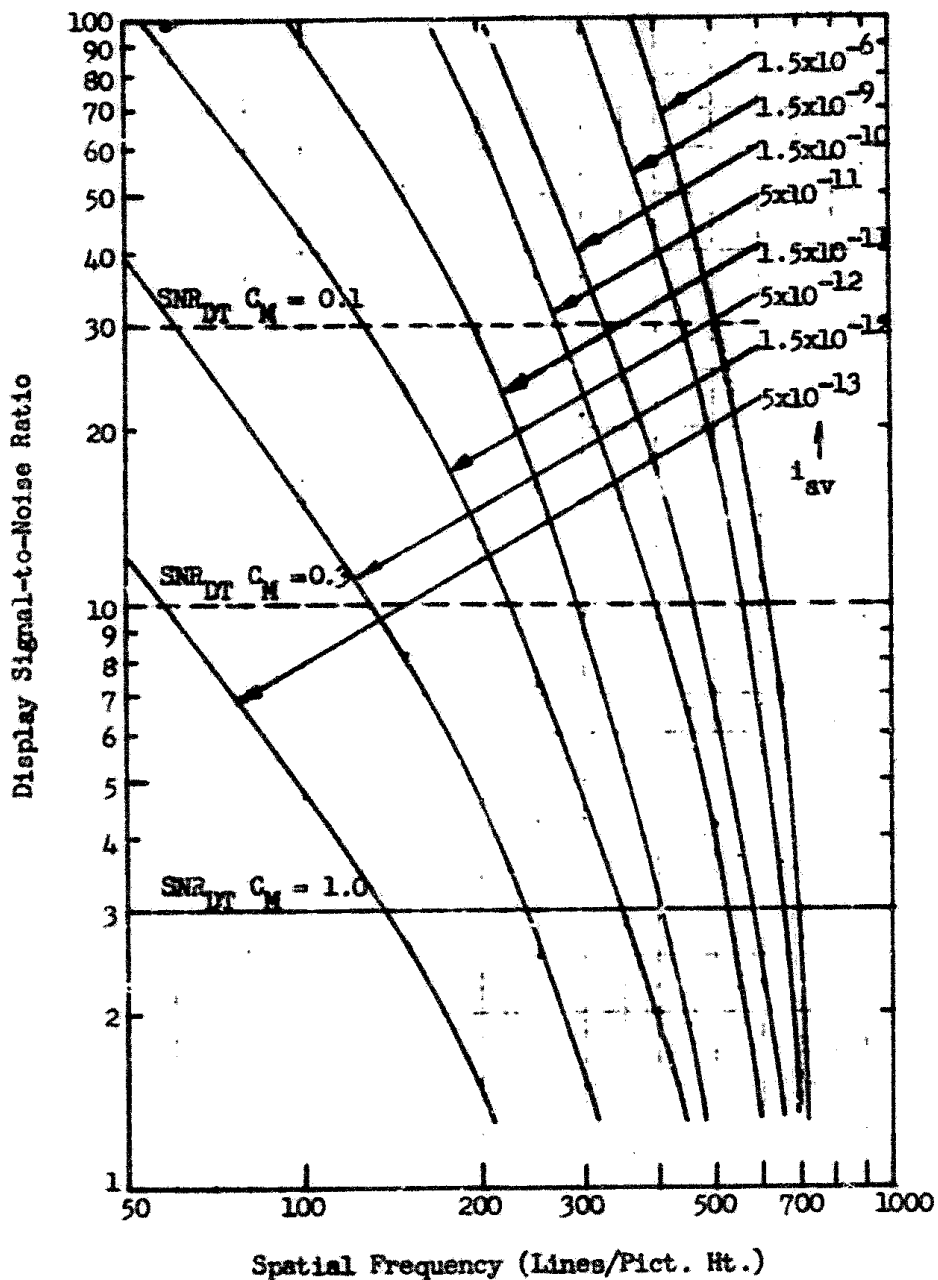


Fig. 7 Display Signal-to-Noise Ratio vs Spatial Frequency for the Assumed System at Various Average Input Photocathode Currents for Bar Pattern Images.

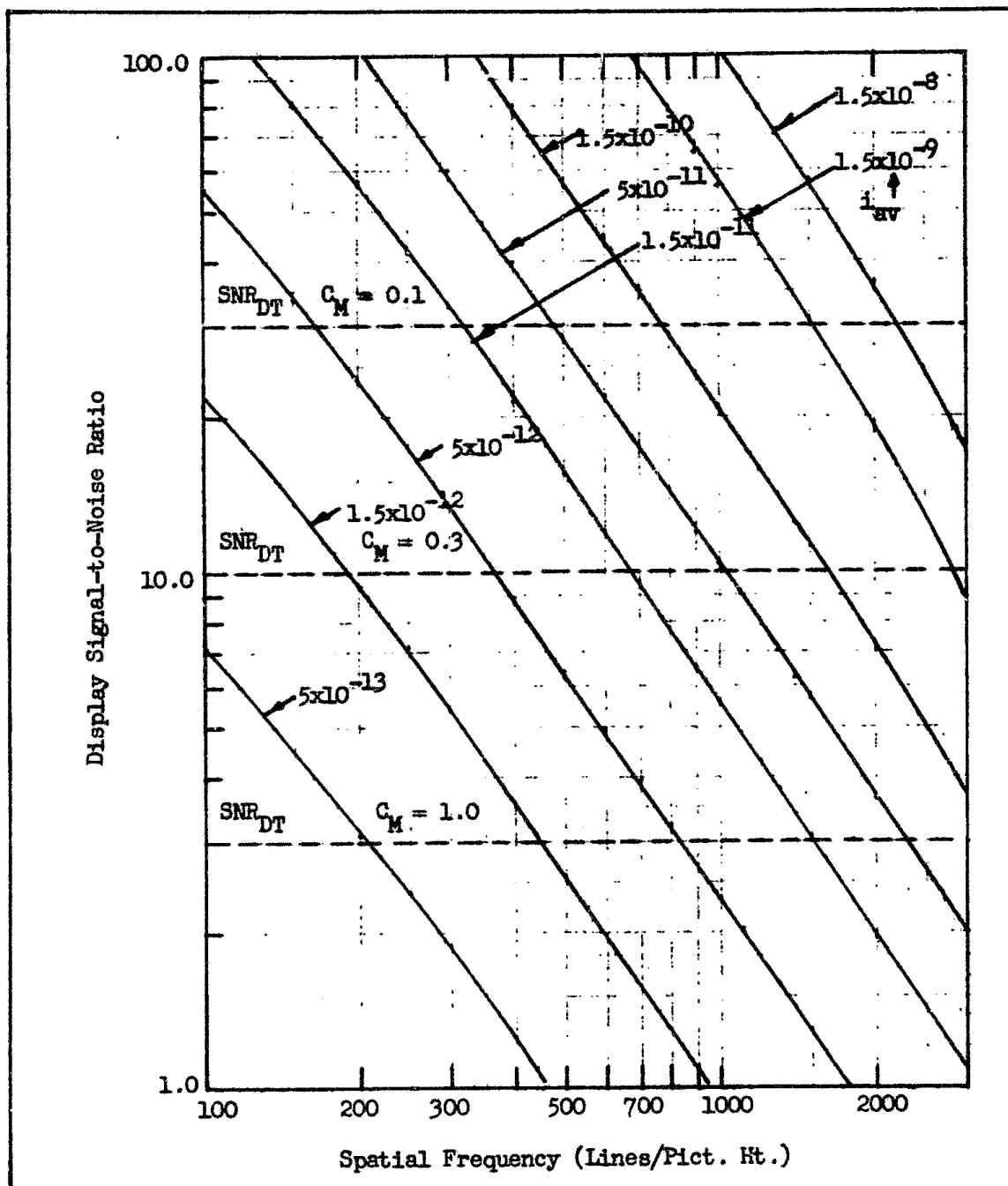


Fig. 8 Display Signal-to-Noise Ratio vs Spatial Frequency for the Assumed System at Various Average Input Photocathode Currents for Aperiodic Images.

resolution vs input photocurrent curves shown in Fig. 9 and 10. The very high resolution numbers associated with the aperiodic objects may appear startling at first, but as will be shown in Section 5, resolutions of the order predicted are in fact realized in real systems. It is seen that the MTF of the sensor has a much smaller effect on aperiodic images than on periodic images.

We have proposed that the system resolution be the average of the resolution calculated on the basis of the aperiodic object and the periodic object. A similar concept has been proposed by Schade (Ref. 4) which he refers to as balanced resolution. Schade notes that aperiodic objects are more frequently observed in nature than periodic objects but he weights the periodic and aperiodic resolution estimates equally as we have tentatively suggested. The method of weighting is considered open to revisions in the future and as discussed in Section 2.5.

Using the balanced resolution concept, the range predicted for sensors will substantially increase. On the other hand, we note that range estimates made previously on the basis of the equivalent bar pattern (or periodic model) seemed to correlate reasonably well with observed ranges in many cases. However, this cannot be construed as an indication of the superiority of the periodic resolution model as opposed to the balanced (aperiodic/periodic) model. The reason for the apparent superiority of the equivalent bar pattern (periodic) approach is that in previous systems analysis it has been usual, more often than not, to ignore a considerable number of image degrading effects including

- 1) sensor time constants

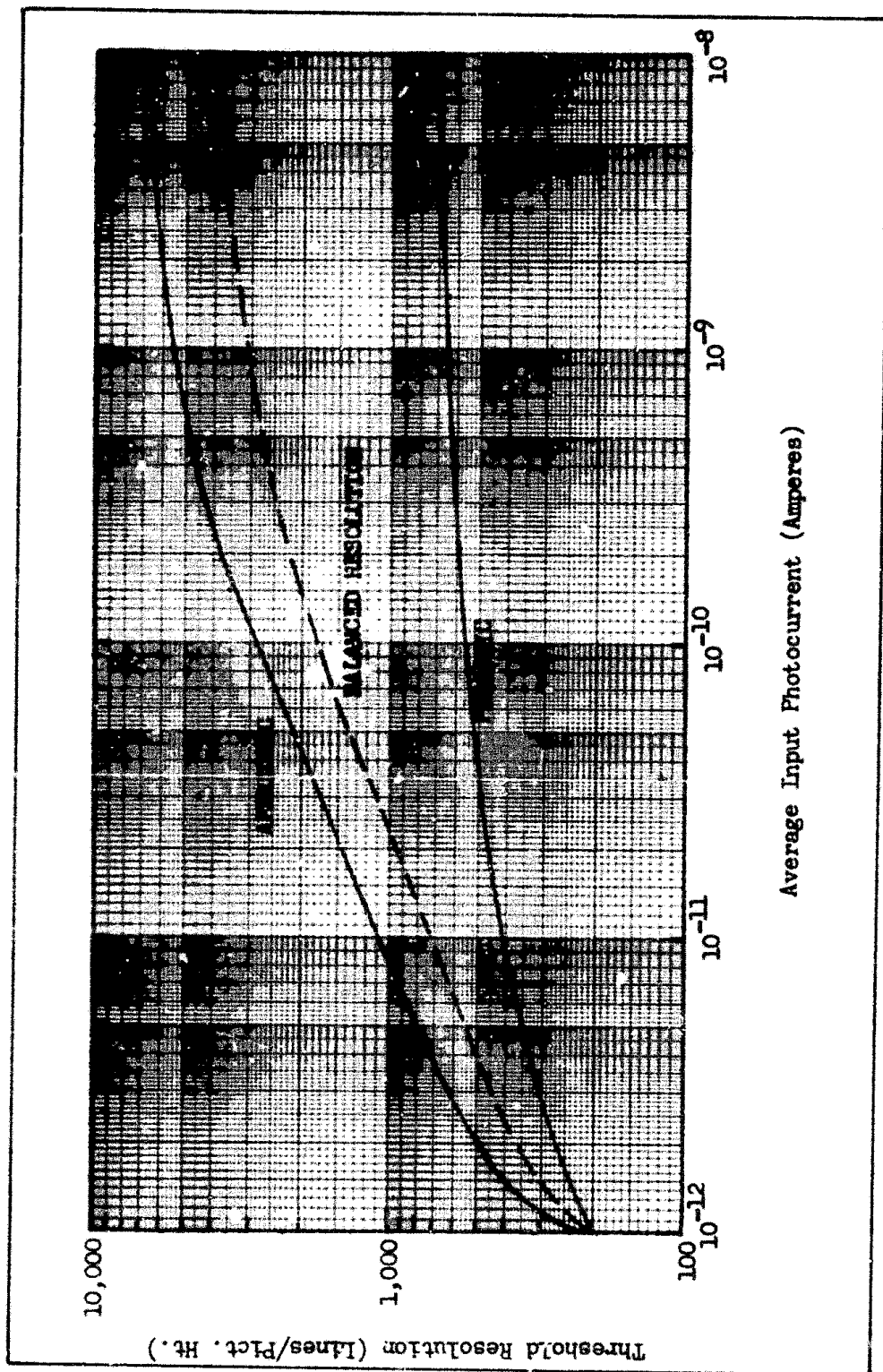


Fig. 9 Threshold Resolution vs Average Input Photocurrent for the Assumed System with Input Image Modulation Contrast of 1.0.

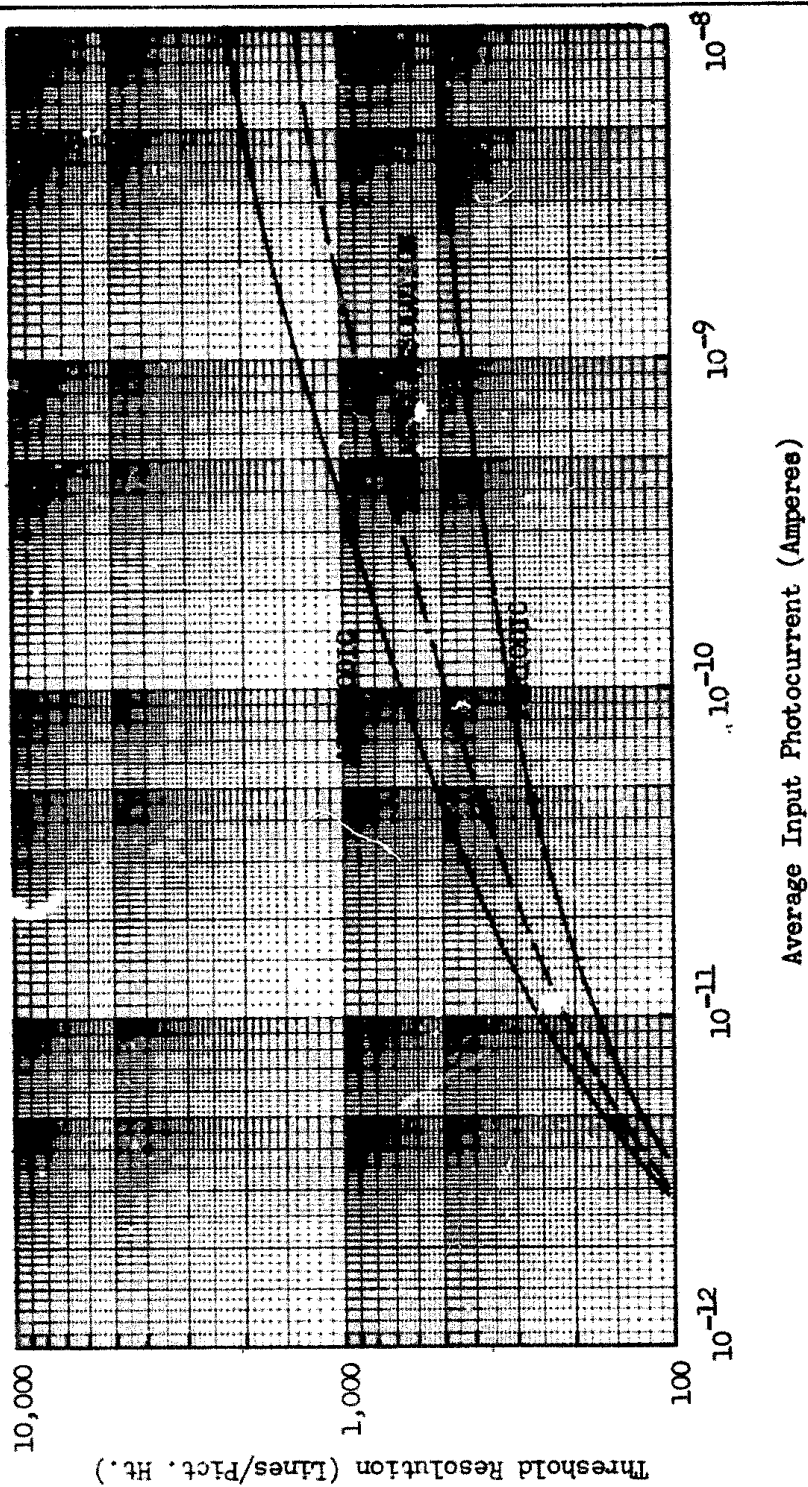


Fig. 10 Threshold Resolution vs Average Input Photocurrent for the Assumed System with Input Modulation Contrast of 0.1.

- 2) line-of-sight instability
- 3) MTF in the vertical direction
- 4) observer limitations
- 5) display dynamic range limitations
- 6) system degradation in the field
- 7) certain MTF losses such as that due to aerodynamic boundary layers, atmospheric turbulence, windows and the like

The point is that the pessimistic nature of the periodic model undoubtedly compensates for the neglect of many other system defects. As we will see, including some of the effects above in the periodic model would cause range predictions to fall far below the ranges measured.

In the above, we have used the input photosurface current as a parameter. This can be related to the input photosurface irradiance through the integral relation

$$i = \int_0^{\infty} \sigma(\lambda) A E(\lambda) d\lambda \quad , \quad (18)$$

where $\sigma(\lambda)$ is the spectral responsivity of the photosurface, A is its effective area, and $E(\lambda)$ is its irradiance. For specific sources, such as a tungsten lamp, sunlight, etc., we can use the approximation

$$i = \sigma_B A E_B \quad , \quad (19)$$

where σ_B is the specific responsivity to a specific source irradiance E_B . We will use this approximation recognizing its limitations.

The average input photosurface irradiance E_{pav} is related to the average scene irradiance E_s through the formula

$$E_{pav} = \frac{\rho_{av} E_s}{4T^2}, \quad (20)$$

for a diffusely reflecting surface of average reflectivity, ρ_{av} , and a lens of T stop = T where T is the ratio

$$T = F_L / D \sqrt{\tau_0}, \quad (21)$$

with F_L equal to the lens focal length, D equal to the lens diameter and τ_0 equal to the lens transmittance.

The sensor resolution is given in terms of "lines per picture height" which, being dimensionless, is a convenience in the sensor analysis since image size can undergo several changes in the various sensor image and reimaging steps. By use of dimensionless units, MTF scale changes need not be made. From a systems viewpoint, the system's threshold angular resolution is of more interest. Knowing the threshold resolution, N , in lines per picture height, the threshold angular resolution, $\Delta\theta$, can be easily calculated using the formula

$$\Delta\theta = \frac{Y}{N \cdot F_L}, \quad (22)$$

where Y is the effective input photocathode height and F_L is the lens focal length. $\Delta\theta$ is interpreted as the angular subtense of a single bar of spatial frequency N .

We averaged the threshold resolutions calculated for the periodic

and aperiodic images as plotted in Fig. 9. Then i_{av} is converted to E_s , the highlight scene irradiance using the combination of Eqs. (19 and 20), i.e.,

$$E_s = \frac{4T^2}{\rho_{av}} \cdot \frac{i_{av}}{\sigma A} \quad (23)$$

In the calculation, the parameters of Table 4 were used. The scene irradiance if given in Watts/m² can be approximately related to an equivalent scene illuminance level given in ft-candles by multiplying the Watts/m² by 2. Finally, the averaged threshold resolution, expressed in angular terms as plotted vs input photocurrent in Fig. 11. The use of angular units has the merit of being independent of the scene object's linear dimensions.

Before proceeding, we note that the gain used in Eqs. (11 and 14) is a variable. For very high scene irradiance levels, the sensor gain is reduced to about 2. As the scene irradiance is reduced, the sensor gain is increased until it reaches its maximum value (2000 for the sensor assumed).

The resolving power of a real imaging system will be degraded by the atmosphere intervening between the scene and observer. The amount of degradation will be primarily a function of the scene-to-camera range, the meteorological visibility, the sky condition and the sky-to-ground brightness ratio. These factors are discussed in some detail in (Ref. 2) but will be briefly reviewed here.

The meteorological visibility is a function of the number and sizes of particles in the air and its effect on scene object detectivity

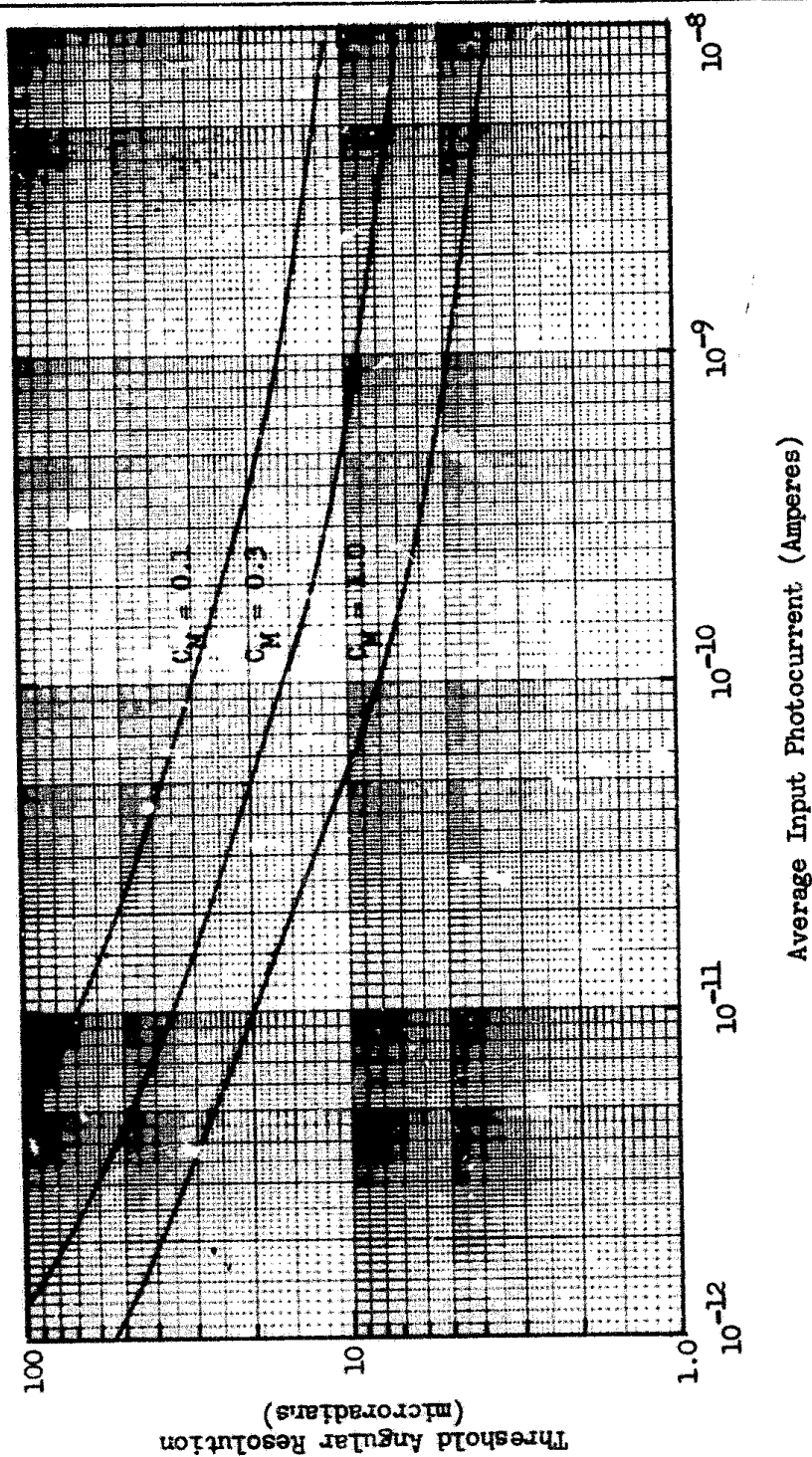


Fig. 11 Threshold Angular Resolution vs Average Input Photocurrent for the Assumed System with Various Input Image Modulation Contrasts. Threshold Resolution is Based on the Balanced Resolution Concept. Angle Corresponds to One Line Width.

is, to a certain extent, a function of the directivity and the type of scene light. Subjectively, the visibility is described by terms such as exceptionally clear, very clear, clear, haze and fog. Semiquantitatively, the visibility is described by the maximum range at which a large black object viewed against the horizon sky becomes barely perceptible when its apparent contrast in the visible spectrum at the observer's location drops to 2%.

For the case of a black object viewed against the horizon sky, the ratio of apparent contrast, i.e., the object's contrast at range, R , to the inherent contrast at range zero, is

$$\frac{C_R}{C_0} = e^{-\sigma R} \quad , \quad (24)$$

where σ is the atmospheric extinction coefficient. The primary effect of the atmosphere in this case is to increase the object's brightness leaving the background (sky) brightness unchanged. In the air-to-ground surveillance case, the atmosphere increases the brightness of both the object and the background so that the equation for contrast reduction becomes

$$\frac{C_R}{C_0} = \frac{1}{[1 - \frac{S}{G}(1 - e^{-\sigma R})]} \quad , \quad (25)$$

where S/G is the ratio of the brightness of the horizon sky to that of the grounds. For a clear sky

$$\frac{S}{G} \sim \frac{0.2}{\rho} \quad , \quad (26)$$

<u>Sky Condition</u>	<u>Ground Condition</u>	<u>S/G</u>
Clear	Fresh Snow	0.2
Clear	Desert	1.4
Clear	Forest	5.0
Overcast	Fresh Snow	1.0
Overcast	Desert	7.0
Overcast	Forest	25.0

Table 5 Typical Values of the Sky-to-Ground Ratio.

where ρ is the background reflectivity. For an overcast sky

$$\frac{S}{G} \sim \frac{1}{\rho} , \quad (27)$$

Middleton (Ref. 5) gives the typical values of Table 5. The case of $S/G = 1$ for the downlook case is identical to the case of viewing an object against the horizon sky. When $S/G < 1.0$, as for fresh snow under a clear sky, contrast degradation is less than for viewing against the horizon sky and conversely, it is greater when $S/G > 1.0$.

Curves of C_R/C_O are shown in Fig. 12 as a function of range for various values of S/G . It is seen that C_R/C_O falls off very rapidly for S/G large. These curves were drawn for a visibility of 10 nmi.

In Table 5, it was noted that with a clear sky and a desert background, $S/G = 1.4$ while with the same background under an overcast sky, $S/G = 7.0$. Assuming a 20 nmi visibility (very clear) C_R/C_O is plotted for $S/G = 1.4$ and 7 in Fig. 13. It is seen that the image contrast, C_R , falls off much more quickly for an overcast sky ($S/G = 7.0$) than it does for a clear sky ($S/G = 1.4$). In both cases, the same scene is being viewed.

Suppose that a bar pattern is used as a test object in the flight evaluation of the equipment. Including the effect of atmospherics, the SNR_D Eq. (14) applies except that

$$C_M = C_{MO} / [1 - S/G(1 - e^{-\sigma R})] , \quad (28)$$

where C_{MO} is the object contrast at zero range. At a given scene light level, the signal, being contrast dependent, becomes range dependent in turn as shown in Fig. 14. With no atmosphere, i.e., a vacuum, the TV camera resolution would be independent of range as shown by the dashed line. With a real atmosphere of 20 nmi visibility, the sensor resolution drops from 620 lines to about 460 lines at 40,000 feet viewing a desert scene under clear sky conditions. Under overcast sky, the resolution drops from 620 to 300 lines. The equivalent curves expressed in terms of angular resolution are shown in Fig. 15. Also, the effect of the atmosphere and the sky-to-ground ratio on other values of contrast are shown in Figs. 16 and 17.

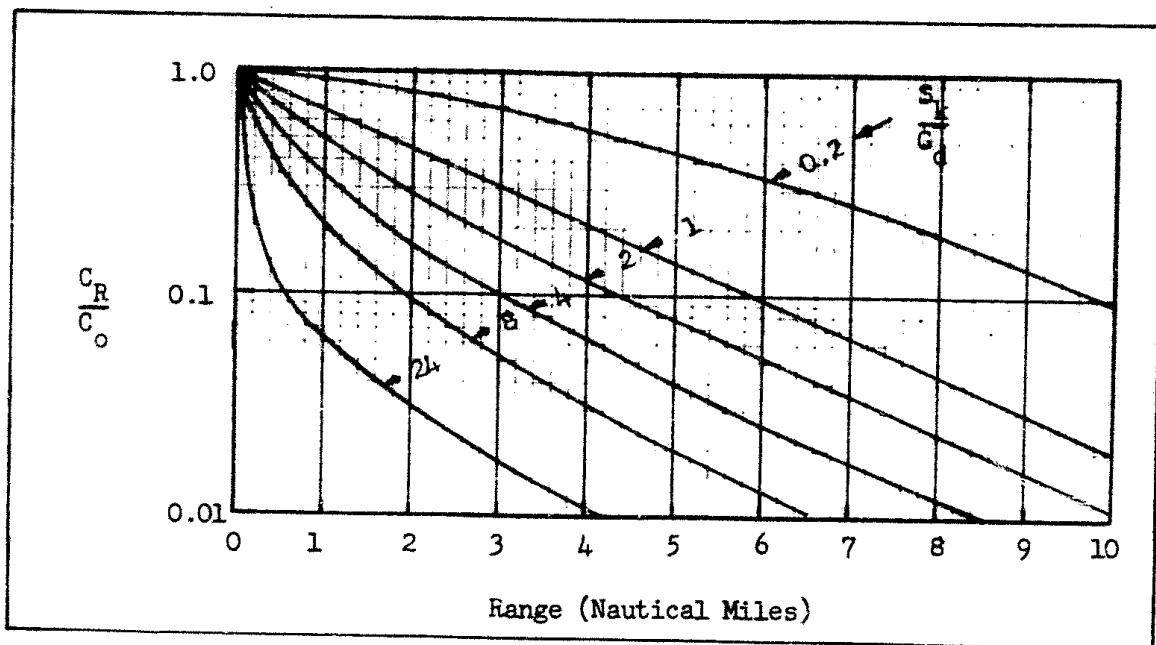


Fig. 12 Ratio of Apparent to Inherent Contrast vs Range for Various Values of Sky-to-Ground Ratio for a Meteorological Visibility of 10 Nautical Miles.

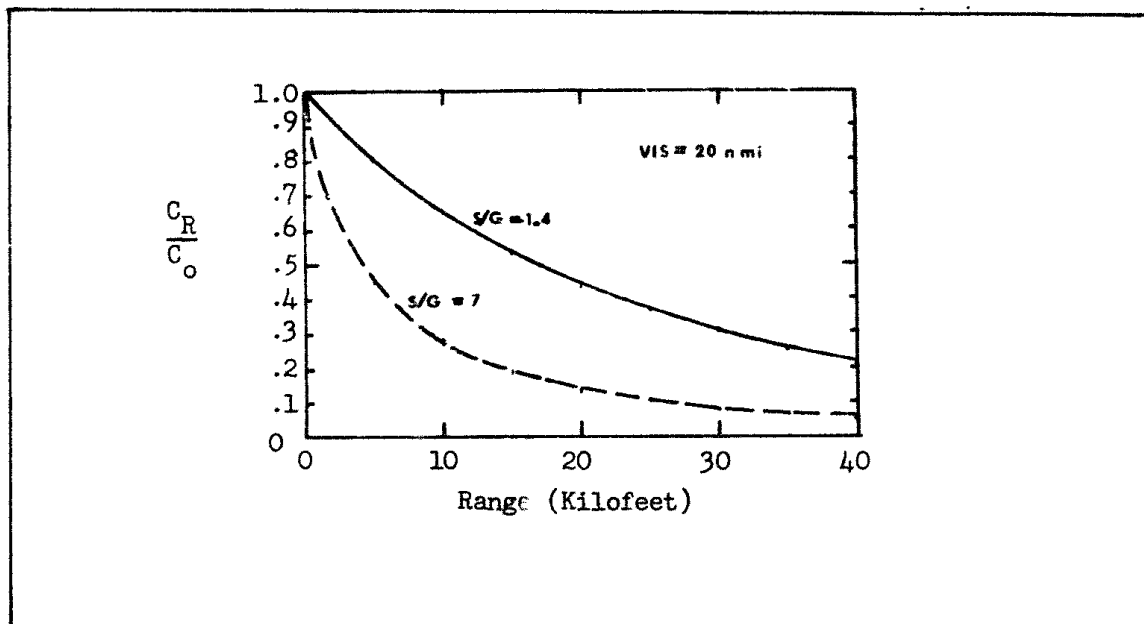


Fig. 13 Ratio of Image Contrast at Range R to that at Range Zero vs Range for a Meteorological Visibility of 20 Nautical Miles and Sky-to-Ground Ratios of 1.4 and 7.0.

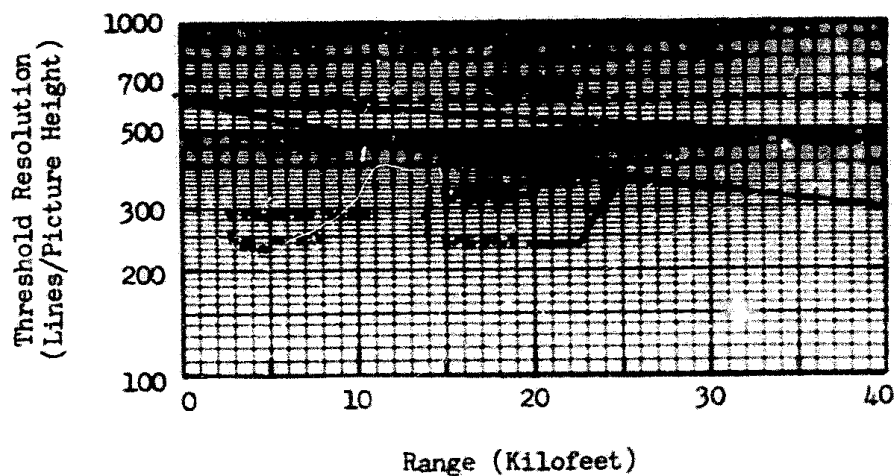


Fig.14 Threshold Resolution vs Range for a Meteorological Visibility of 20 Nautical Miles and Sky-to-Ground Ratios of 1.4 and 7.0.

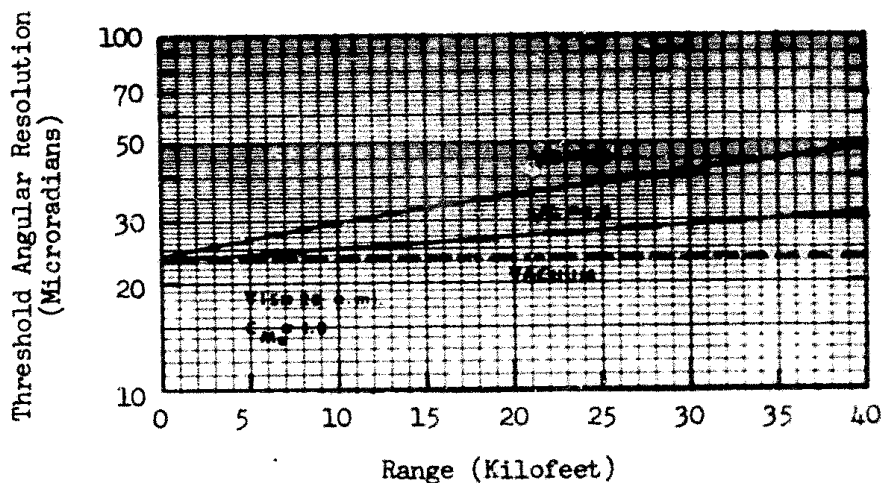


Fig.15 Threshold Angular Resolution vs Range for a Meteorological Visibility of 20 Nautical Miles and Sky-to-Ground Ratios of 1.4 and 7.0.

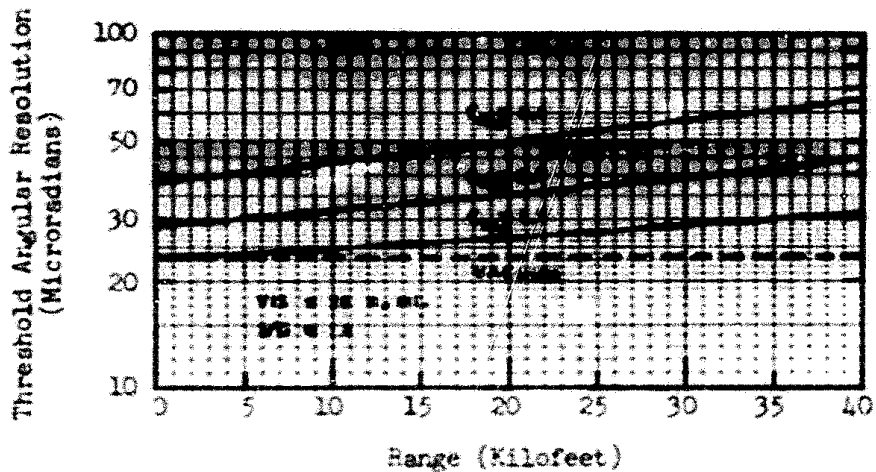


Fig. 16 Threshold Angular Resolution for Bar Patterns vs Range for the Assumed TV Camera as a Function of Input Image Contrast for a 20 nmi Visibility and a Sky/Ground Ratio of 1.4.

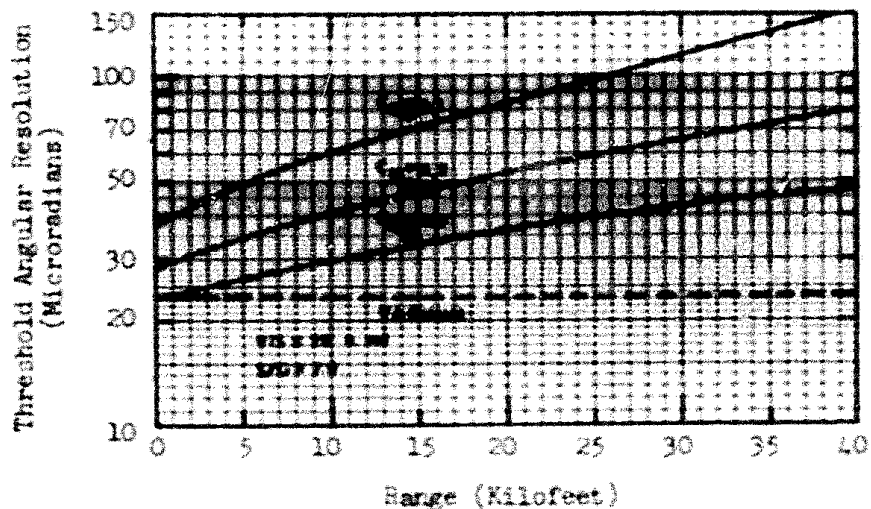


Fig. 17 Threshold Angular Resolution for Bar Patterns vs Range for the Assumed TV Camera as a Function of Input Image Contrast for a 20 nmi Visibility and a Sky/Ground Ratio of 7.0.

The atmosphere may also have a modulation transfer function due to thermal gradients, inversion layers, etc. These are most serious for ground based TV telescopes but do affect air-to-ground viewing as well. These effects are noted but not analyzed further herein.

2.3 Active Television Imaging Systems

An active imaging system is one which images a scene lighted by an auxiliary system source. In the case of interest here, the auxiliary source is located near the television telescope. A simple search light qualifies as an auxiliary source but the trend in recent sophisticated systems is to use a pulsed laser which may be range gated to eliminate atmospheric backscatter. The analysis of active television systems of the range gated variety has been treated in some detail in Ref. 2 but will be reconsidered using the updated model.

The system parameters will be identical to those considered in the previous section with the primary change being the addition of a 40 watt system source (sometimes called an illuminator), an image intensifier and an electronic exposure gate for the TV camera. The system source is of the GaAs variety which provides 0.85 micron radiation in 2 μ s bursts. The photoresponse of the input photocathode is taken to be 2.5×10^{-2} A/W and the intensifier gain is presumed to be 20 (ratio of current in the TV camera tube to that in the intensifier). For first order analysis, The Eqs. (11 and 14) will be used as for the passive case. The principal differences from a systems viewpoint are that the inherent scene contrasts will tend to be higher, the atmosphere will have a much smaller effect on the apparent scene contrast but may severely decrease scene irradiance.

An active system, used only during the night hours, will usually be limited by a low scene irradiance and photoelectron noise rather than by preamplifier noise as is the case for a daylight system. Since light levels are low, the designer of an active system seeks high sensitivity and low sensor lag rather than a large signal storage capability as the daylight system designer does.

The actual scene irradiance is given by the relation

$$E_s = P_o \exp(-\sigma R) / \omega R^2, \quad (29)$$

where P_o is the source power (watts), σ is the atmospheric extinction coefficient, ω is the solid angle irradiated (sr), and R is the slant range from camera to scene. The average sensor irradiance level assuming a diffuse scene is obtained from

$$E_{pc} = \frac{\rho_{av} P_o \exp(-2\sigma R)}{4T^2 \omega R^2}, \quad (30)$$

where ρ_{av} is the average scene reflectivity and T is the lens T/stop (equal to the lens f-number divided by the square root of the lens' transmittance). Note that the atmosphere decreases the scene irradiance on both its trip to the scene and its return. The input photosurface current, i_{av} , is given by

$$i_{av} = \frac{\rho_{av} S A P_o \exp(-2\sigma R)}{4T^2 \omega R^2}, \quad (31)$$

where S is the photosurface responsivity (A/W) and A is its effective area. The above photocurrent is plotted in Fig. 13 for 3 values of

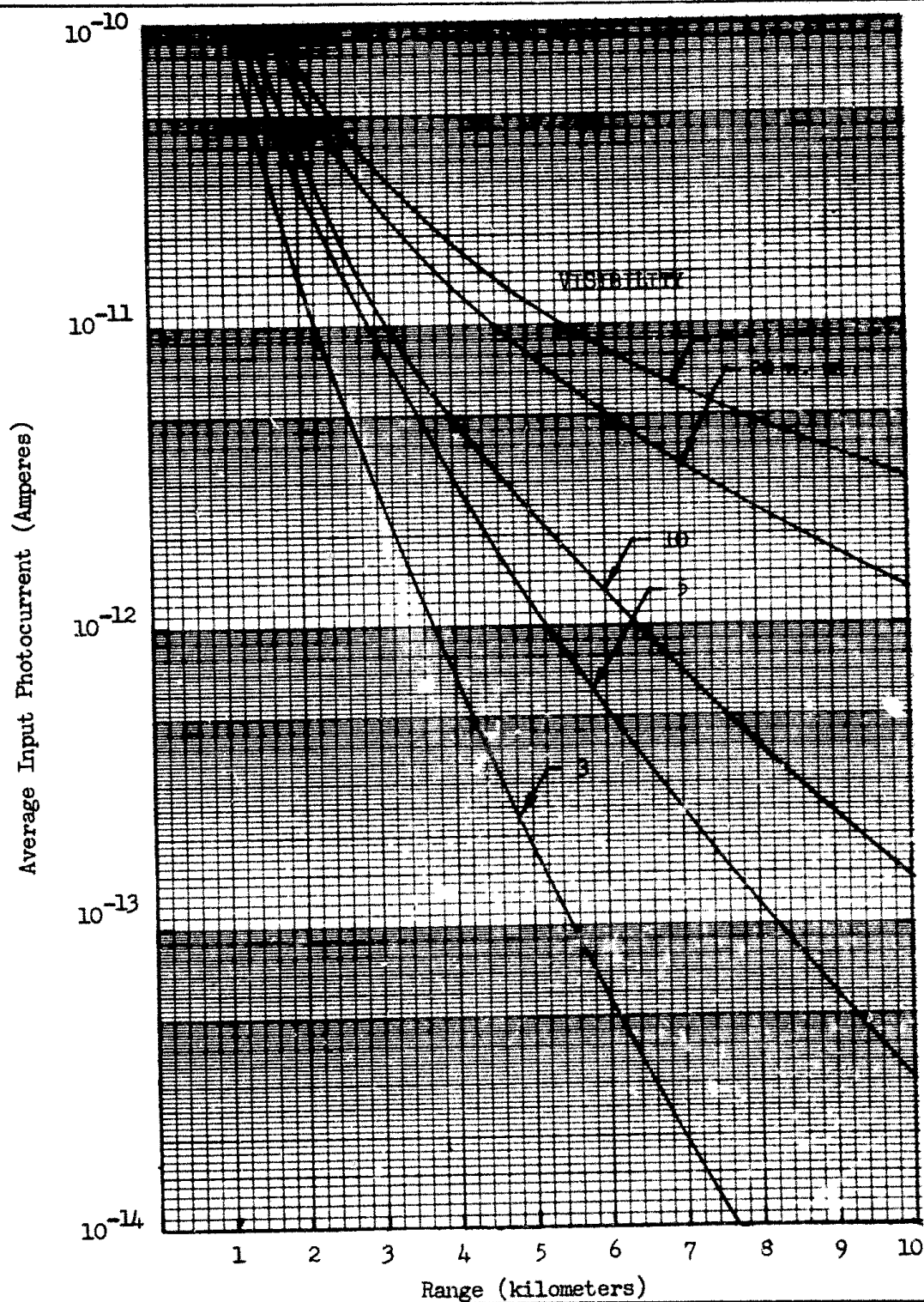


Fig. 18 Average Input Photocurrent for the Assumed System vs Range for an Average Scene Reflectivity of 0.3.

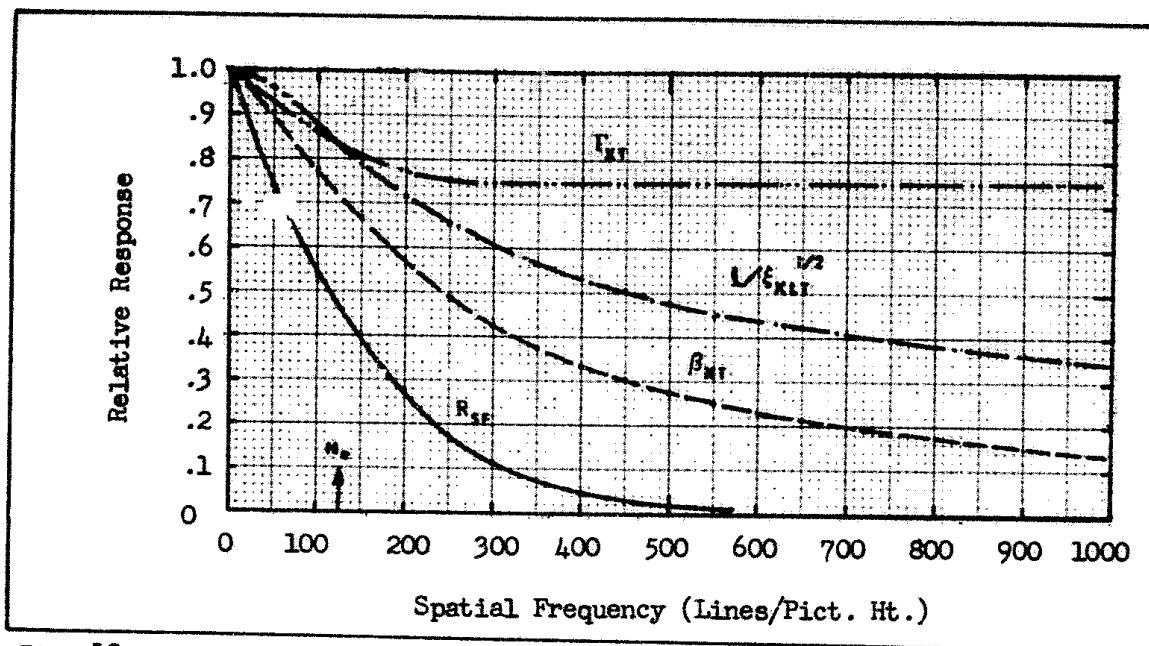


Fig. 19 MTF and MTF Related Quantities for the 16/16/16 mm I-EBSICON Camera Used in the Assumed System.

visibility, (sea level, horizontal path assumed). From these curves, it is possible to make some resolution vs range estimates directly. A typical 16 mm I-EBSICON camera tube, operated at full gain saturates with input photocurrents near about 5×10^{-11} Ampere. For high scene contrasts, it is possible to image with currents as low as 10^{-13} A while, for moderately low contrasts, 10^{-12} A may be required. For the moderately low contrast case, the range at which a reasonably good image will be obtained will vary from about 3.5 to 15 kilometers depending upon the visibility.

The MTF and MTF related quantities are shown in Fig. 19. As can be seen, the intensifier has an appreciable effect on the overall square wave flux response. Because of the high gain of the intensifier and camera tube ($\sim 40,000$), the Eqs. (11 and 14) reduce to

$$\text{SNR}_D = \left[\frac{t\varepsilon}{\alpha} \right]^{\frac{1}{2}} \cdot \frac{1}{N} \cdot \frac{2C_M(i_{av})^{\frac{1}{2}}}{[e\xi_{xLT}(N)\Gamma_{xT}(N)\xi_{yLT}(N)\Gamma_{yT}(N)]^{\frac{1}{2}}} \quad (32)$$

for aperiodic objects and for periodic objects

$$\text{SNR}_D = \left[\frac{t\varepsilon}{\alpha} \right]^{\frac{1}{2}} \cdot \frac{R_{SF}(N)}{N} \cdot \frac{2C_M(i_{av})^{\frac{1}{2}}}{[e\xi_{yLT}(N)\Gamma_{yT}(N)\beta_{xT}(N)]^{\frac{1}{2}}} \quad (33)$$

These SNR_D values are plotted in Figs. 20 and 21 for an inherent object contrast of 0.5 and a meteorological visibility of 20 n. miles. The meteorological visibility determines the average photocurrent as given by Eq. 31. The threshold resolution vs range is plotted in Fig. 22 in terms of bar pattern spatial frequency and in terms of angular subtense of a single bar in Fig. 23. It is seen that the aperiodic resolution dominates as was noted in the passive imaging case but the difference between periodic and aperiodic resolution is not as pronounced. Note that as range increases, the resolution predicted on the periodic model basis approaches that predicted on an aperiodic model.

In the above, we neglected the loss of image contrast due to a finite laser pulse width and a finite range gate interval. These effects are discussed in some detail in Ref. 2.

2.4 Effects of Image Motion

We have seen that the resolution of scene detail can be limited by the ambient light level, system generated noises and by the atmosphere. To these limitations, we now add relative scene motion. The effects of image motion are to cause the image to blur in a manner analogous to the blur caused by an added system aperture. Indeed,

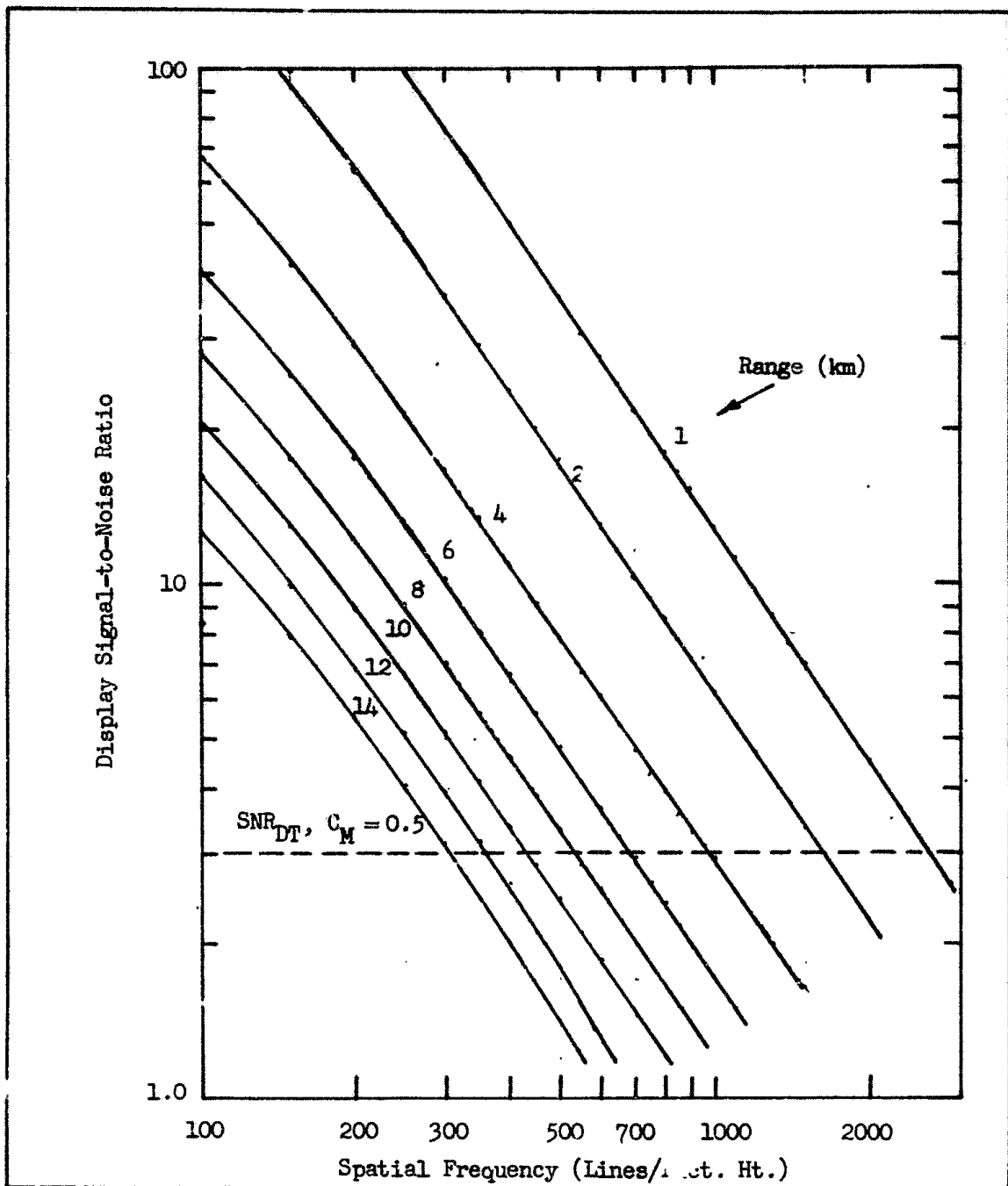


Fig. 20 Display Signal-to-Noise Ratio vs Spatial Frequency for the Assumed Active System for an Inherent Image Contrast of 0.5 and a Visibility of 20 n. mi. Calculations are based on the Aperiodic Image Model.

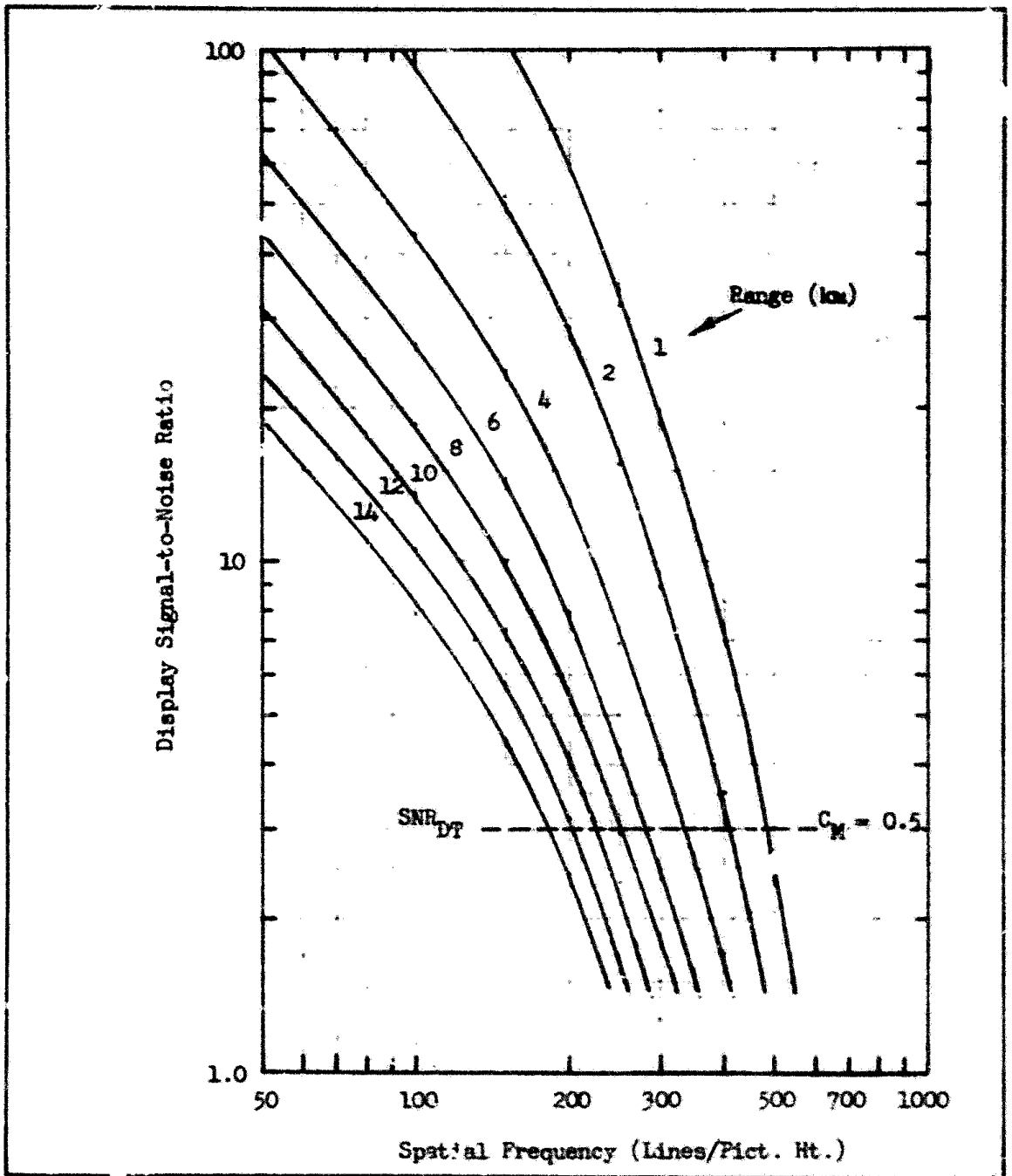


Fig. 2i Display Signal-to-Noise Ratio vs Spatial Frequency for the assumed Active System for an Inherent Image Contrast of 0.5 and a Visibility of 20 n. mi. Calculations Based on the Periodic Image Model.

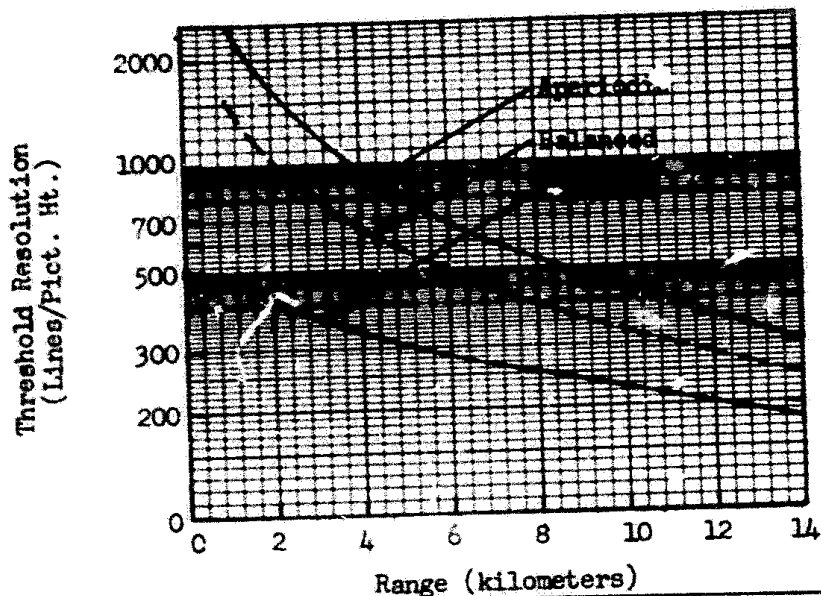


Fig. 22 Threshold Resolution in Lines/Pict. Ht. for the Assumed Active System vs Range. Inherent Image Contrast is 0.5.

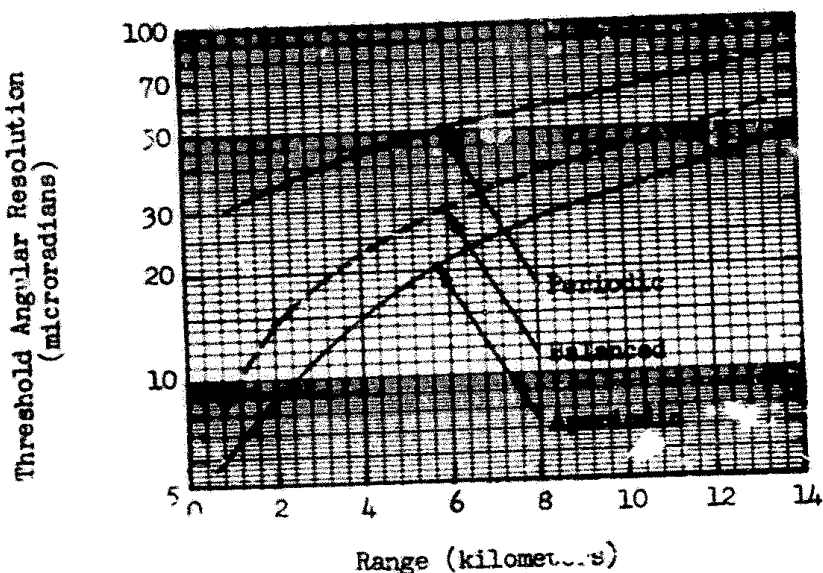


Fig. 23 Threshold Resolution in Angular Subtense of a Single Line vs Range for the Assumed Active System. Inherent Image Contrast is 0.5.

motion effects can often be described in terms of a modulation transfer function.

One effect of image motion is to induce image lag effects due to the TV system's read-in and read-out time constants. These effects are light level dependent; being most pronounced at the lower light levels. We shall consider these effects following the discussion of the effects of exposure time.

Relative scene motion may be caused by machinery within the TV camera enclosure (such as blowers or pumps) by noise in motion sensors such as gyros, by platform perturbations such as aircraft vibration or by the forward motion of the platform as occurs in flight. This relative image motion is a problem because the TV camera has an exposure time.

Typically, the television camera has an exposure time of $1/30$ second although, under high light levels, the effective exposure time may be reduced to near the field time of $1/60$ second. This reduction in effective exposure time is due to the readout of both fields by the electron beam during a single scan of the charge storage surface. The result is low resolution pictures, presented displaced by one line from one field to the next. The resultant picture resolution is higher than that of either field alone but probably not as high as it would be if the picture on each field were independent from the other. These effects have been noted but lack quantitative measure. For the purposes of this discussion, the TV exposure time will be assumed to be $1/30$ second unless otherwise noted.

Except for the usual effects due to scanning, the exposure or frame time of a television camera is directly analogous to the exposure time of

a photographic camera. A photographer, taking even stationary scene pictures, must be very careful to avoid jiggling his camera when using exposure times of the order of $1/30$ second. Ordinarily, he will prefer to use $1/100$ to $1/200$ second exposure times to avoid camera motion problems. When photographing action scenes, exposure times are usually reduced further to about $1/500$ second or less. It is noted that the effect of image blur due to relative scene or camera motion may be worse for a single photographic exposure than it is for cinematography or for television where several blurred pictures, slightly displaced, may combine in the observer's eye to form an overall image of greater clarity as in the television case where both fields are readout in a single field as discussed above. Again, these effects have not been quantitatively investigated to the author's knowledge.

Given a stationary camera, the relative scene motion is a function of the distance of the scene from the camera. It is clearly more difficult to photograph a 60 mph car passing across the camera viewfield at a range of 10 feet than it is at 1000 feet. In the usual airborne reconnaissance system, ranges are very long -- typically, 5000 to 50,000 feet and the scene motion is relatively negligible. However, the camera's line-of-sight is continually being perturbed by the aircraft's velocity, the ambient vibration of environment, and the mechanisms required to slew, point and stabilize the line-of-sight. In general, the line-of-sight will be in continuous motion of some kind. Even when a ground point is being perfectly tracked, only one point in the image will be stationary -- all other points in the viewfield will be in relative angular motion. Many of these effects have been discussed in considerable detail in Ref. 2.

Consider an aircraft in straight and level flight. Let a TV camera view the ground with a fixed depression angle. Then the line-of-sight to the fixed ground point will rotate as the aircraft flies toward it. The image of the point will travel from the bottom of the picture to the top. For changes in the sightline which are not too large, the rate of image motion is approximately linear. Alternatively, the line-of-sight may oscillate about the ground point with reasonably constant amplitude and frequency due to mechanical resonances, or oscillate with random amplitudes and frequencies due to noises generated by the inertial sensors or due to other noises transmitted by the mechanical structure.

The eye can track scene objects which are moving at very high angular rates compared to the angular rates which the television camera will tolerate without losing significant scene resolution. Thus, for our purposes, we can concentrate on the motion-induced sensor effects. It is also clear that to blur an image, the image's motion must be comparatively large during an exposure time. However, the term large is relative to the size of the image detail to be resolved. The amount a small object can move without being blurred beyond recognition is also small.

The effects of image motion on scene resolution has been analytically treated for a number of simple but quite common cases (Ref. 6). These are linear motion, sinusoidal vibration of constant amplitude, and sinusoidal vibration of random amplitude. These will be discussed below. As one would intuitively expect, linear motion is the least degrading and random motion is the most.

In photographing or televising an object passing across a field of view, a sharp picture will be obtained only if the angular rate of

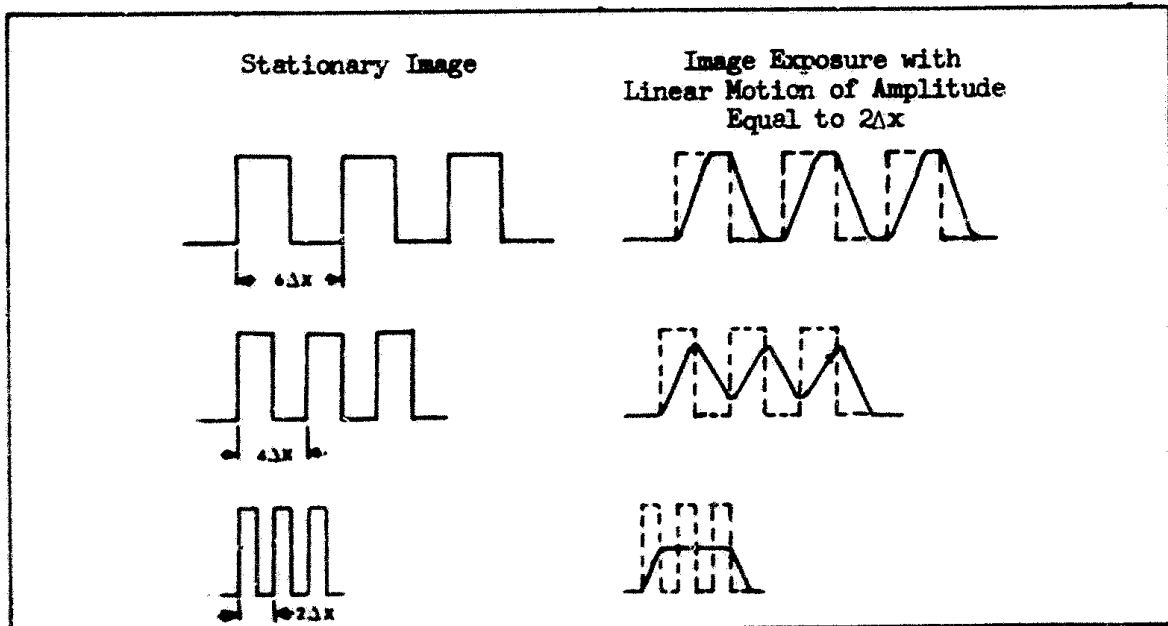


Fig. 24 Effect of Image Motion on Bar Patterns of Various Spatial Frequencies.

the object is small relative to the object's angular detail during the exposure time. As the object's angular rate increases, the object's image begins to blur with fine details being the first to disappear. Suppose that the object is a bar pattern as shown in Fig. 24. If the coarse pattern of period $6\Delta x$ moves a distance $2\Delta x$ during an exposure time, the intensity waveform in the exposed image, though of the same amplitude, becomes trapezoidal. If the bar pattern spacing becomes smaller, so that the period is $4\Delta x$, the exposed image's amplitude within the bar pattern is reduced and the waveshape tends toward sinusoidal. With a bar pattern of period equal to the distance moved during the exposure time, i.e., $2\Delta x$, the exposed image becomes a uniform grey, i.e., there is no modulation in the exposed image and the bar pattern structure disappears.

It is customary in TV engineering to express the image resolution

at the input photocathode in terms of a spatial frequency with units of lines per picture height. That is, if the bar (or sine wave) spacing is Δx (period of $2\Delta x$) and if the picture height is Y , then the spatial frequency, N , is equal to

$$N = \frac{Y}{\Delta x} \frac{\text{lines}}{\text{picture height}} \quad (34)$$

By analogy with the above discussion, it is seen that if the image motion is 2 lines in an exposure time, then the output image modulation becomes zero.

As shown in Ref. 2, the effect of linear image motion can be described in terms of a modulation transfer function given by

$$R_o(N) = \frac{\sin(\pi N v_i t_f / 2Y)}{\pi N v_i t_f / 2Y} \quad (35)$$

for v_i equal to the pattern speed in mm/sec, Y equal to the picture height and t_f equal to the frame or exposure time. In laboratory measurements, it is common to specify the bar pattern velocity in terms of the number of seconds, t_s , required for one bar in the test pattern to traverse the field of view. Using this specification, the pattern velocity becomes

$$v_i = \frac{4Y}{3t_s} \quad (36)$$

(for a picture aspect ratio of 4/3). Now,

$$R_o(N) = \frac{\sin(2\pi N t_f / 3t_s)}{2\pi N t_f / 3t_s} \quad (37)$$

This MTF is plotted in Fig. 25 for various pattern velocities. The

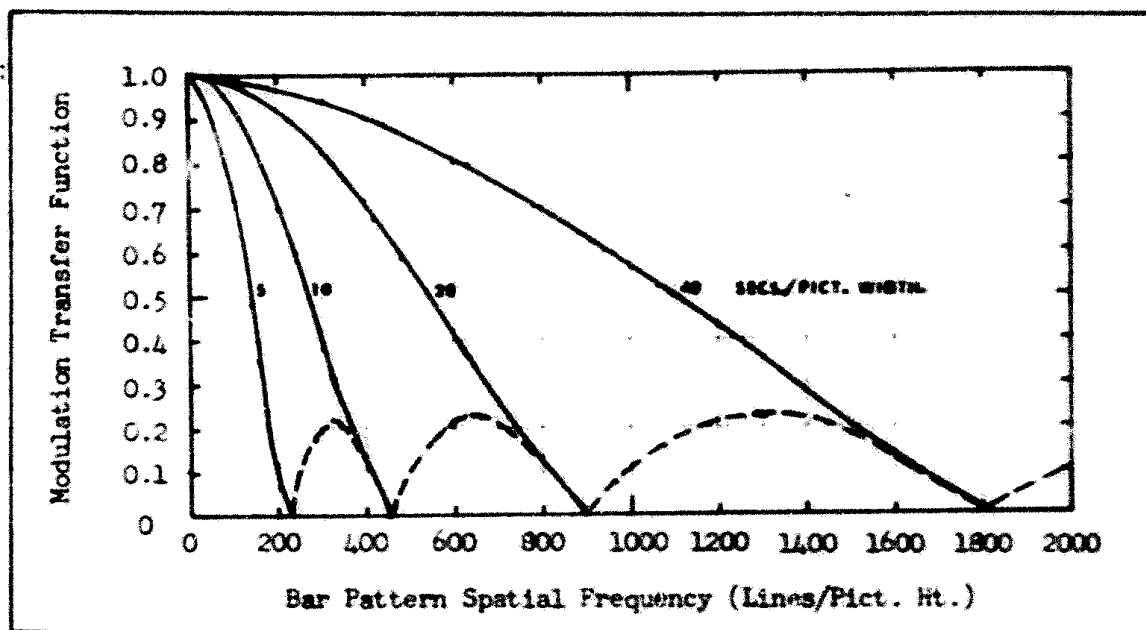


Fig. 25 Modulation Transfer Function Due to Linear Image Motion Plotted to Second Zero for Various Bar Pattern Velocities Expressed in Terms of Time for Pattern to Traverse Picture Width.

response is seen to go to zero and then increase again as shown by the dashed lines. The increase in response after the first zero results when the bar pattern motion exceeds 2 lines/exposure time. The response is negative indicating a phase reversal, i.e., the black lines appear as white on the display and conversely. While a signal modulation results, it is not generally useful and is called false resolution. The spatial frequency at which the response first goes to zero is given by

$$N_c = \frac{3}{2} \frac{t_s}{t_f} \quad (38)$$

and is plotted in Fig. 26. The angular motion per frame time corresponding to N_c is also plotted in the same figure for the assumed daylight system of Section 2.2.

If it is desired to resolve a certain spatial frequency, say 225

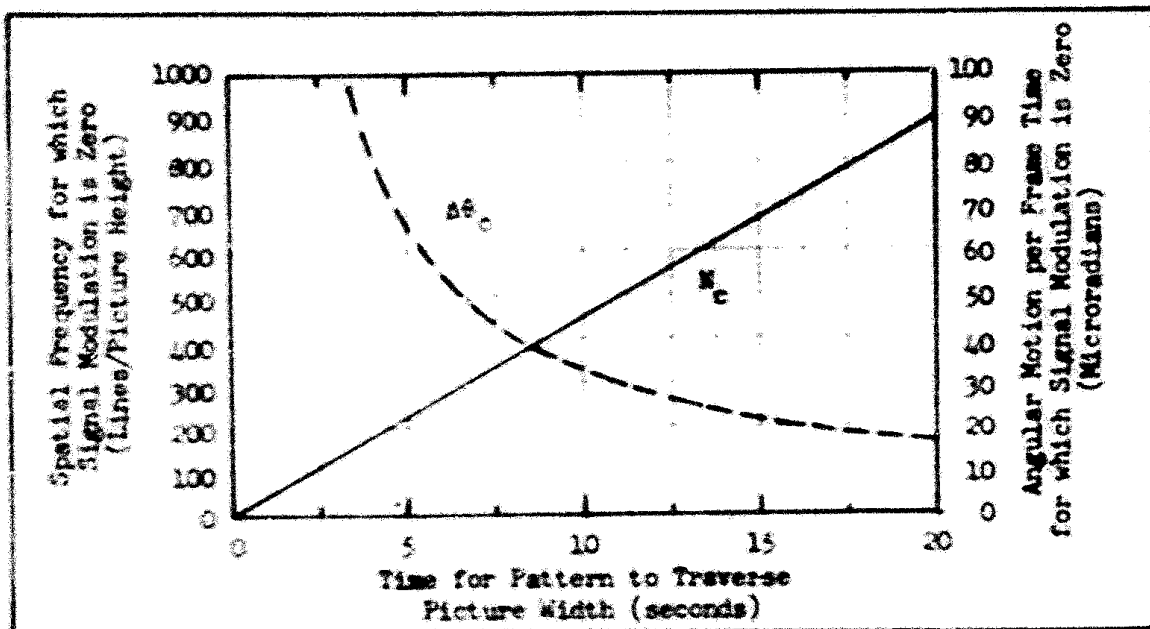


Fig. 26 Spatial Frequency and the Corresponding Angular Motion for the Assumed System for which the Signal Modulation is Zero as a Function of Bar Pattern Motion (Linear).

lines, the pattern velocity must be less than 5 seconds per picture width, for at that velocity, the signal modulation decreases to zero. How much less, depends upon the loss in signal modulation that can be tolerated. For example, if the MTF must be 0.5 or better at 225 lines, the cut-off frequency N_c must be increased. In Fig. 27, we plot MTF vs N/N_c . For 0.5 response, N/N_c is about 0.6 and thus to obtain 0.5 response at $N = 225$ lines, N_c must be increased to $225/0.6$ or 375 lines and the motion from Fig. 26 must be less than about 8.5 sec/picture width.

In yet another description, we let $\Delta x_v = v_f t_f$ be the distance moved per exposure time and since $\Delta x = l/N$, then

$$\begin{aligned}
 R_o(N) &= \frac{\sin(-\Delta x_v / 2\Delta x)}{-\Delta x_v / 2\Delta x} \\
 &= \frac{\sin(-\pi v_f / 2)}{-\pi v_f / 2}
 \end{aligned} \tag{39}$$

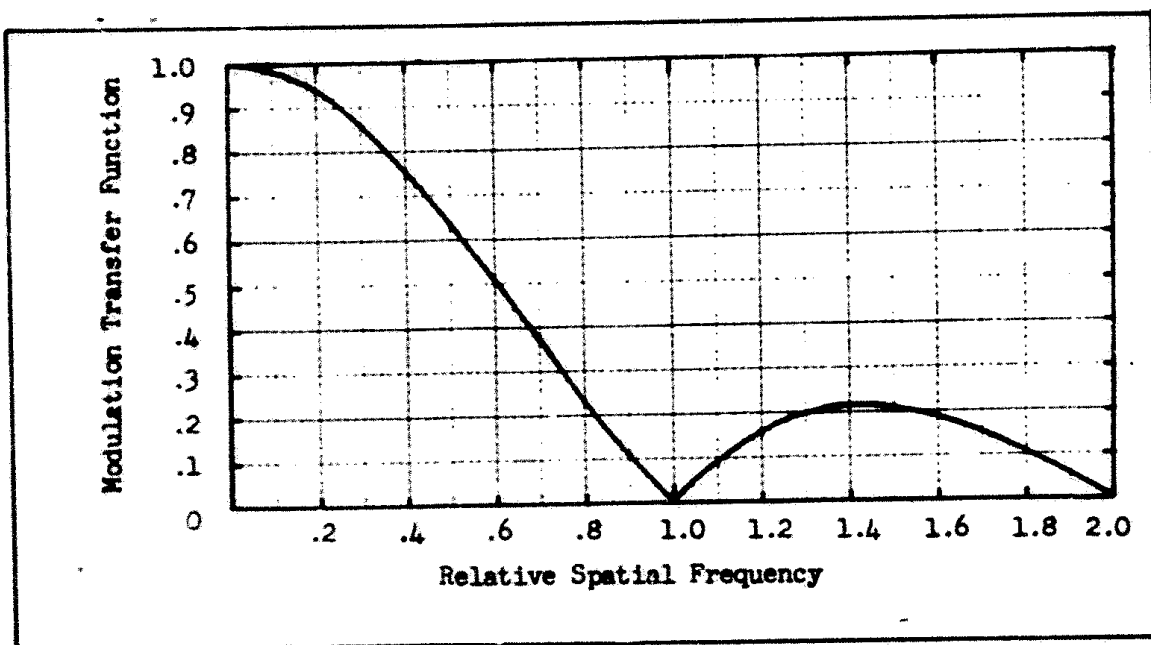


Fig. 27 Modulation Transfer Function Due to Linear Image Motion vs Spatial Frequency Normalized to the Cut-Off Frequency.

where n_v is the number of lines the pattern moves in an exposure time. This MTF is plotted in Fig. 28. It is seen that if the bar pattern moves one line per integration time, the MTF drops to 63% while for $1\frac{1}{2}$ lines, the MTF is 29%.

In most air-to-ground surveillance tasks, a ground point must be quite precisely tracked. The linear motion MTF argument can be used to conclusively show this need. Assuming a ground point is tracked, linear motion should not be much of a factor but its discussion is still worthwhile because it is the easiest to understand.

Sinusoidal image motion of constant amplitude can result from resonances in the mechanical structure. The form of the motion is shown in Fig. 29. The MTF for sinusoidal motion has been derived

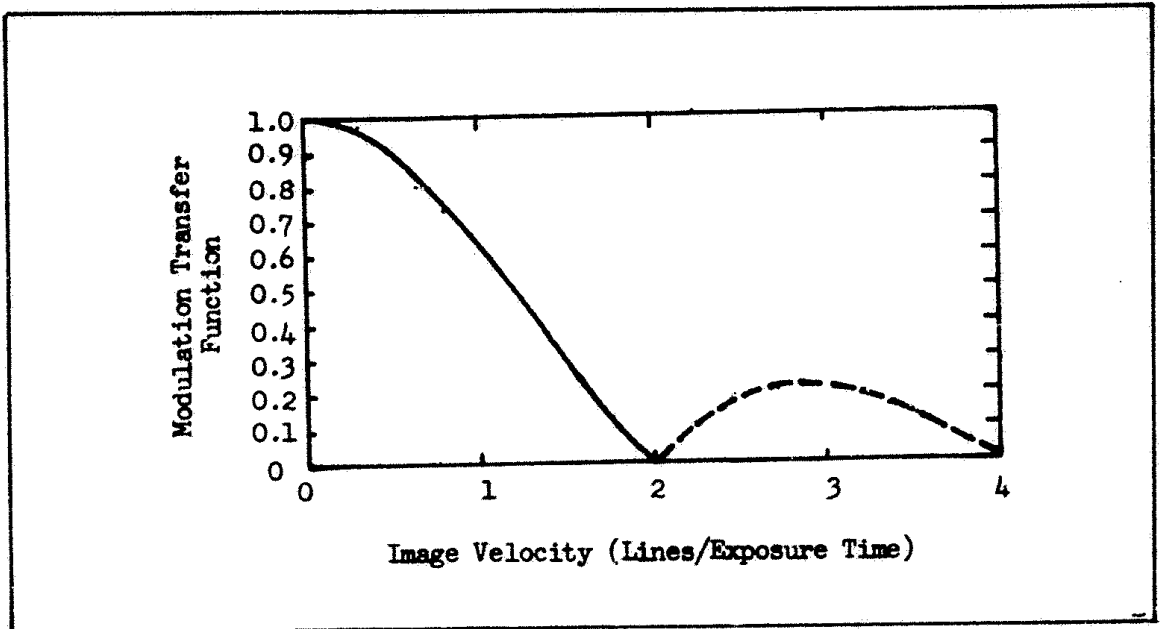


Fig. 28 Modulation Transfer Function for Linear Image Motion.

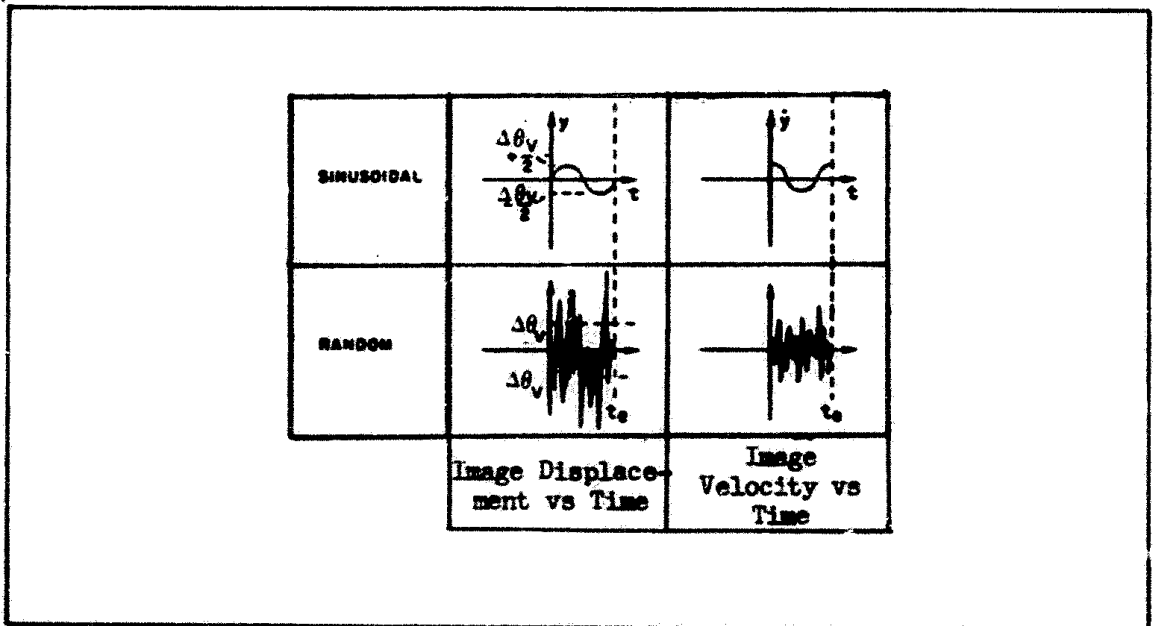


Fig. 29 Waveforms of Image Displacement and Velocity vs Time.

for the special case where the beginning of a cycle coincides with the beginning of the exposure time and ends at the end of the exposure time. The effect will be the same whether one cycle or an integral number of cycles occur within the exposure time — the MTF is a function only of the spatial frequency of the sinusoid and its amplitude. The MTF is

$$R_0(N) = J_0\left(\frac{AN}{2Y}\right), \quad (40)$$

where J_0 is a Bessel function of zero order, A is the peak-to-peak amplitude of the motion in mm and Y is the picture height also given in mm. For the assumed system, the amplitude, A , may be written as $F_L \cdot \Delta\theta_v$ where F_L is the lens focal length and $\Delta\theta_v$ is the peak-to-peak angular motion. Then,

$$R_0(N) = J_0\left(\frac{\pi F_L \Delta\theta_v N}{2Y}\right). \quad (41)$$

This function is plotted in Fig. 30 for $\Delta\theta_v = 25, 50$ and 100 microradians. Again, a negative (false resolution) response can be discerned.

Next, we note that the cutoff spatial frequency, i.e., the spatial frequency at which the response goes to zero in Fig. 30 is given by

$$N_c = 1.53 N_v, \quad (42)$$

where N_v is the amplitude of the motion measured in lines per picture height. Alternatively, in angular terms

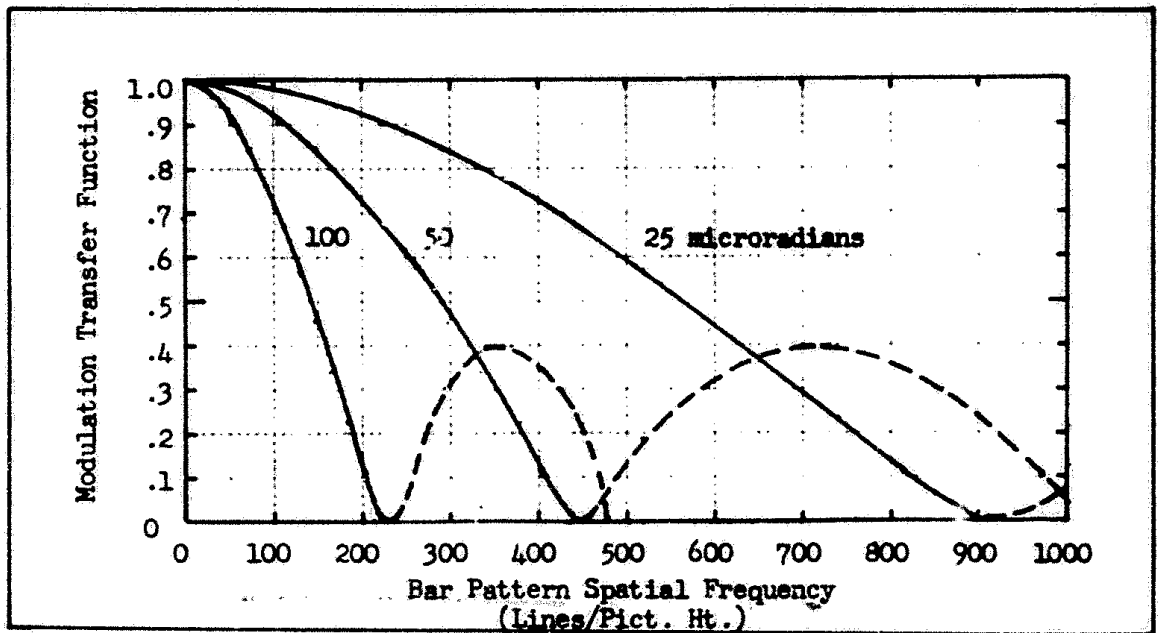


Fig. 30 Modulation Transfer Function vs Bar Pattern Spatial Frequency for Sinusoidal Motion of Peak Amplitude of 100, 50 and 25 microradians per Exposure Time for the Assumed System.

$$\Delta\theta_c = \frac{\Delta\theta_v}{1.53} , \quad (43)$$

and

$$N_c = \frac{Y}{F_L \cdot \Delta\theta_c} = \frac{1.53Y}{F_L \cdot \Delta\theta_v} . \quad (44)$$

These last two functions are plotted in Fig. 31. To illustrate, suppose the peak-to-peak sinusoidal motion is 100 microradians per exposure time. Then $\Delta\theta_c$, the angular subtense of a bar in the bar pattern for which the signal modulation is zero is 62.8 microradians. For our assumed system, 62.8 microradians translates to a TV camera resolution of 222 lines per picture height.

In normalized form, the modulation transfer function becomes

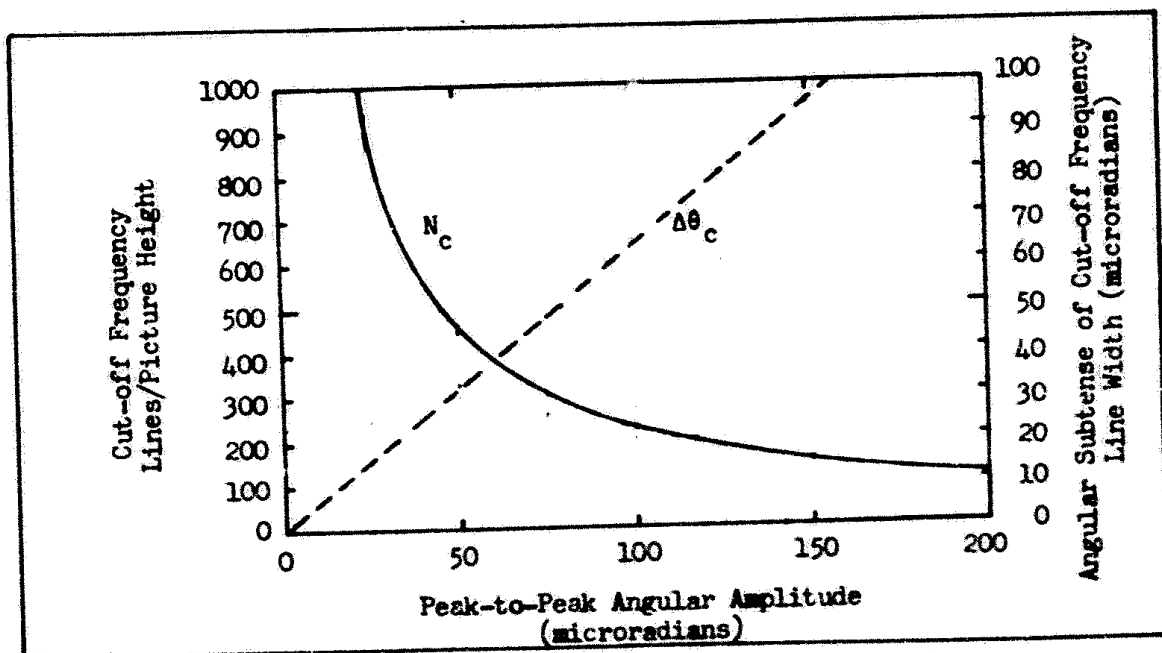


Fig. 31 Cut-off Frequency and the Angular Subtense of Cut-off Frequency Line Width vs the Peak-to-Peak Angular Amplitude of Sinusoidal Motion.

$$R_o(N) = J_o\left(\frac{1.53\pi}{2} \cdot \frac{N}{N_c}\right) \quad (45)$$

which is plotted in Fig. 32. This curve can be used in a manner analogous to Fig. 27 to determine the value of the modulation transfer factor at a spatial frequency below the cutoff value.

Finally, the modulation transfer function is shown in Fig. 33 as a function of the peak-to-peak motion given in terms of the number of lines the motion subtends at the spatial frequency in question. It is seen that if the bar pattern motion is 1 line per exposure time, the MTF drops to 47% and drops to zero for motion of the order of 1.5 lines per exposure time.

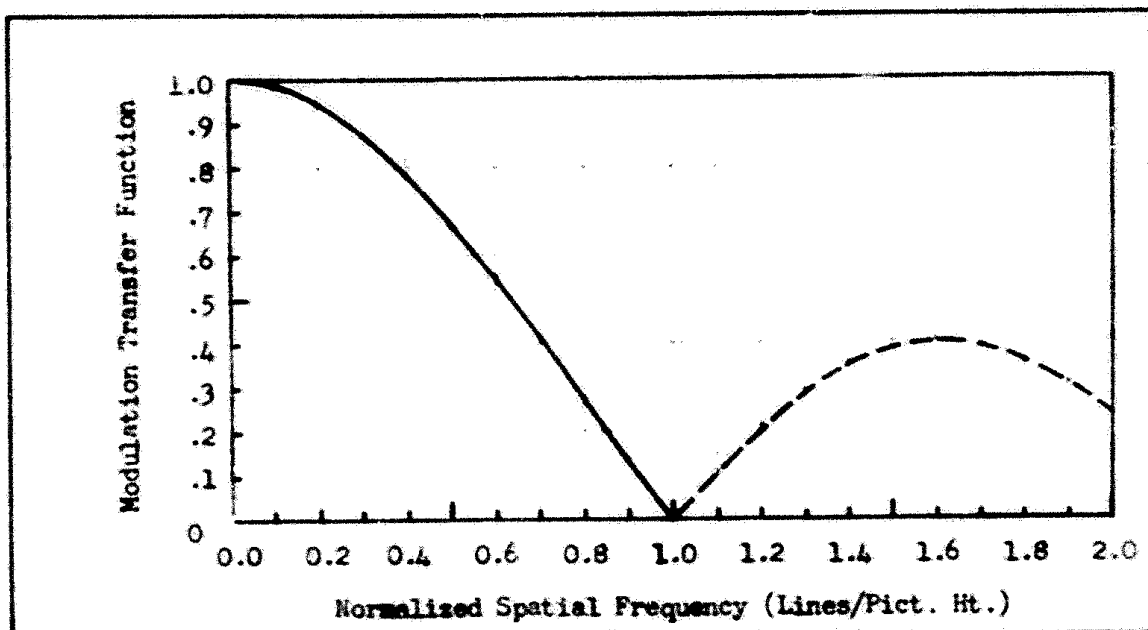


Fig. 32 Modulation Transfer Function for Sinusoidal Motion vs Spatial Frequency Normalized to the Cut-off Frequency.

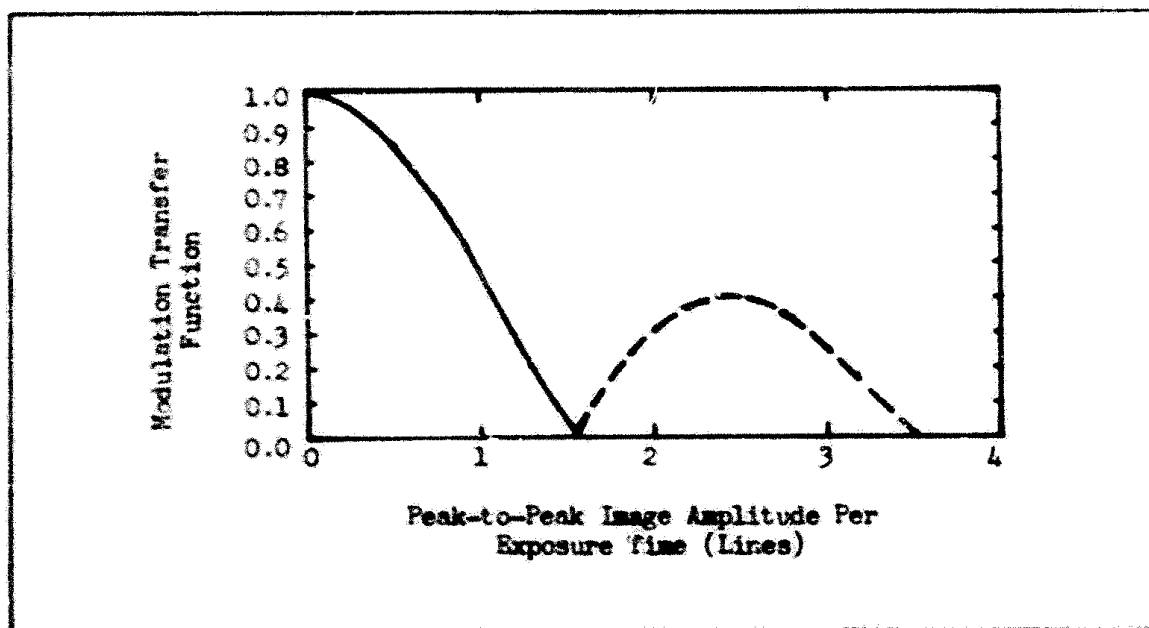


Fig. 33 Modulation Transfer Function for Sinusoidal Image Motion.

It is seen in Fig. 30 that image motion of any particular spatial frequency has an effect at all other spatial frequencies. It may happen that the line-of-sight will vibrate at 2 or more frequencies (or be such that it can be decomposed into a small number of discrete frequencies). In this case, the overall MTF effect can probably be estimated by taking the product of the MTF's associated with the various frequencies.

Random motion is perhaps the most commonly encountered in practice. For this case, the MTF is given by

$$MTF = \exp\left[-\frac{1}{2}\left(\frac{\pi AN}{Y}\right)^2\right] \quad (46)$$

with the terms being as before except that the amplitude, A , is measured in terms of its rms value. As in the sinusoidal motion case, we can write the amplitude A as $F_L \Delta\theta_v$ so that

$$MTF = \exp\left[-\frac{1}{2}\left(\frac{\pi F_L \Delta\theta_v N}{Y}\right)^2\right] \quad (47)$$

This equation is plotted in Fig. 34 for various values of the angular motion amplitude $\Delta\theta_v$.

Since the exponential term does not pass through zero, we arbitrarily define the cut-off spatial frequency as that frequency for which the MTF is 0.02, then

$$N_c = 0.89 N_v \quad (48)$$

where N_v is the rms amplitude of the motion per frame time measured in